AN INSIGHT INTO THE REACTIONS OCCURRING DURING THE CHEMICAL ACTIVATION OF BONE CHAR

Unai Iriarte-Velasco[a], Jose L. Ayastuy[b], Lorena Zudaire[a] and Irene Sierra[a*]

a Department of Chemical Engineering, Faculty of Pharmacy, University of the Basque Country UPV/EHU, Paseo de la Universidad, 7, 01006 Vitoria, Spain.

b Department of Chemical Engineering, Faculty of Science and Technology, University of The Basque Country UPV/EHU, Barrio Sarriena, s/n, 48940 Leioa, Spain.

*Corresponding author. Tel.: +34 945013290; fax: +34 6015963. Email: irene.sierra@ehu.es

Abstract

The valorisation of animal wastes by pyrolysis has shown to be of interest, due to the versatility of the main compound of char, hydroxyapatite (HAP), which can be used in catalysis, electrochemistry, and adsorption. The utility of HAP depends to a great extent on its textural properties, which can be developed by chemical activation, through gasification reactions. In the present work thermogravimetric analysis coupled to mass spectrometry was used to gain insight into the reactions occurring during the chemical activation of pork bone char with different agents: H_3PO_4, H_2SO_4, NaOH and K_2CO_3. Moreover, the role of each activation reagent in the enhancement of porosity was determined. The treatment with H_2SO_4 resulted in a highly microporous material, suitable to be used in gaseous pollutant adsorption. Chemical activation with NaOH and K_2CO_3, on the contrary, led to a more equilibrated increase of micro- and mesoporosity, resulting in a hierarchical porous material, with an excellent potential for applications as electrode, in gas storage, catalysis and energy storage. Regarding H_3PO_4, it was extremely aggressive under the operating conditions used, since it removed almost all the porous structure of HAP. These results are useful to optimize the preparation method of HAP, in order to configure a material with the desired textural properties.

KEYWORDS: Hydroxyapatite; Bone char; Chemical activation; Reaction mechanism; Mass spectrometry; Thermogravimetry.

1. Introduction

As a result of Bovine Spongiform Encephalopathy crisis, the use of meat and bone meal (MBM) to feed cattle was forbidden in EU (Commission Decision 94/381/EC). Therefore, today there is a high amount of animal wastes that must be safely disposed or transformed. The combustion of MBM and its co-incineration with coal has been studied as a suitable way for energy valorisation [1, 2] and [3]. Nevertheless, the incineration of MBM gives way to a high level of emissions of dioxins and furans [4], and also NO_x, due to the nitrogen content of MBM [5].

Pyrolysis constitutes one of the most reliable treatment methods for the animal bones left over. The solid fraction obtained (char) contains about 70-76 wt% calcium hydroxyapatite (HAP) $Ca_{10}(PO_4)_6(OH)_2$, 9-11 wt% carbon and 7-9 wt% $CaCO_3$. There are other minor constituents, such as calcium sulphate (0.1-0.2 wt%) and Fe_2O_3 (less than 0.3 wt%) [6]. Due to its chemical structure HAP has been recently reported as a very useful material in catalysis [7] and [8], electrochemistry [9] and adsorption [10], [11], [12] and [13] processes.

Spain is the world's fourth largest pork producer, with 3.5 MTn of pigmeat produced in 2012 [14]. Consequently, the preparation of HAP-based materials from pork bone is a promising alternative, given that this process is economically feasible and environmentally friendly.

The utility of HAP depends to a great extent on its textural properties. Chemical activation has been reported as a suitable method to develop a material with high porosity, which is associated with the occurrence of gasification reactions [15]. Moreover, chemical activation has several advantages over physical activation, such as: (i) higher yield; (ii) higher surface area; (iii) better development of porous structures; and (iv) the requirement of lower pyrolysis temperatures [16]. Its main drawback is the need for washing to remove the residual inorganic material.

Several efforts have been made to understand the reactions that take place during the preparation of highly textured materials by chemical activation, using different carbonaceous precursors and activating agents. Senneca [1] studied product distribution during the thermal activation of MBM. Guo et al. [17] studied the chemical activation of oil-palm stone with H_2SO_4 and KOH. Lillo-Ródenas et al. [16, 18] investigated the

reactions occurring during the chemical activation of an anthracite with NaOH and KOH. Robau-Sánchez et al. [19] proposed a reaction mechanism for the activation of Quercus agrifolia char with KOH. Nevertheless, the literature concerning the preparation of porous hydroxyapatites by the chemical activation of animal wastes is scarce, and there are important gaps in the fundamentals of the process, regarding the reaction mechanisms occurring during the heat treatment.

In this work thermogravimetric analysis coupled to mass spectrometry was used to gain knowledge on the chemical activation process of pork bone char with different agents: H_3PO_4, H_2SO_4, NaOH and K_2CO_3. The objectives of this work are: i) Identify the reactions between the constituents of bone char and the activating agents that take place during the preparation of porous hydroxyapatite. Furthermore, since carbon is one of the constituents, the results will help to better understand the fundamentals of the chemical activation process of any carbonaceous precursor. ii) Investigate the effect of the activation process on the physicochemical properties of the final product, in order to optimize the preparation method, resulting in the achievement of a HAP-based material with the desired textural properties.

2. Experimental

2.1 Production of bone char

Bone char (BC) was prepared from pork chop bones collected from a local butcher's shop. The preparation protocol was as follows: first, bones were cleaned from meat and cut into pieces of 2–5 cm. It is known that the evaporation of low molecular weight organic compounds and the decomposition of collagen occurs below 450 ºC [20]. In this way, in order to remove meat and fat, prior to chemical activation bones were precarbonized at 450 ºC, which is about half of the temperature used in the subsequent carbonization step. From now on, precarbonized sample will be referred as precursor. Precarbonization was performed using a heating rate of 10 ºC/min until the desired temperature was reached; temperature was then held constant for 1 hour. Nitrogen flow was set at 120 cm^3/min, which corresponds to 8 minutes of residence time in furnace. Precarbonized samples were left to cold down in nitrogen atmosphere.

The precursor was sieved and particles in the 0.25 – 0.35 mm size range were used. The precursor was divided into five parts. Four were impregnated with H_3PO_4 (P), H_2SO_4

(S), NaOH (N) or K_2CO_3 (K). The activation reagents were supplied by Panreac with laboratory grade purity, H_3PO_4 (86%), H_2SO_4 (96%), NaOH pellets (97%) and anhydrous K_2CO_3 (99%). The last sample was not further modified to be used as a reference (O).

The impregnation ratio was established at 20 mmol of activation agent per gram of precursor (precarbonized bone char). These values are within the normal range used for the chemical activation of other low cost precursors [21], [16], [15] and [22], and ensure sufficient interaction between the activation agent and bone char matrix. For the impregnation step about 2 g of precursor were contacted with 40 cm^3 of a solution containing 1 mol/L of the activating agent. Solutions were introduced in 50 mL borosilicate amber glass vials with Teflon tap and stirred at 120 rpm in a reciprocating shaker at room temperature (20 ± 2 ºC) for 24 h, to ensure the access of the activating agent to the interior of the particles. Samples were then filtered, transferred to a convection oven and dried at 80 ºC for 24 hours. The impregnated materials were coded according to the activating agent used: BCP, BCS, BCN, BCK and BCO.

Finally, impregnated samples were pyrolysed at 800 ºC under operating conditions similar to those used during the precarbonization stage. Samples of BC were washed with distilled water until neutral pH of solution was reached, and their physicochemical properties were measured.

2.2 TG-MS study

In order to investigate the reactions occurring during the activation process, thermogravimetric analysis (TG) coupled to mass spectrometry (MS) was conducted. TG analysis was performed with a Setsys evolution (Setaram) thermal analyser. About 40 mg of sample (BCP, BCS, BCN, BCK and BCO) were put into the ceramic crucible and heated under helium atmosphere from room temperature to 1000 ºC, at a heating rate of 10 ºC/min. The thermal analyser exhaust gases were analysed on-line by a mass spectrometer (MKS, Cirrus 3000). The total pressure in the analysis chamber was 10^{-6} Torr. The following compounds were monitored continuously: H_2 (m/z = 2), CH_4 (m/z = 16), H_2O (m/z = 18), CN^- (m/z = 26), HCN (m/z = 27), CO (m/z = 12), aldehydes (m/z = 29) and CO_2 (m/z = 44). MS signals were normalized by dividing by the signal of He used as carrier.

2.3 Physicochemical characterization

The physicochemical properties of the final samples (chemically activated at 800 ºC) were investigated. Textural properties were determined by nitrogen adsorption/desorption at 77 K, using a porosimeter (ASAP 2010, Micromeritics). Prior to the measurements samples were dried and outgassed at 200 °C under a nitrogen flow for 15 hours. BET surface area, and pore area and volume were measured. Micropore surface and volume were measured from density functional theory (DFT), while values in the mesopore and macropore ranges were determined based on the Barrett, Joyner & Halenda (BJH) method.

The chemical composition and textural structure were analysed by a scanning electron microscope (JEOL JSM-7000F) equipped with energy dispersive X-ray detector (EDX). Fourier-transformed infrared (FTIR) spectra were collected using a Nicolet Protégé 460 device in the transmittance mode, in the 400-4000 cm^{-1} range with a resolution of 2 cm^{-1}. The KBr self-supported pellet technique was used to collect the spectra. The X-ray powder diffraction (XRD, PANalytical Xpert PRO) analyses were performed with CuKα radiation (λ = 1.5418 Å) in continuous scan mode in the 5-70º 2θ range, with a 0.02º step size. The analysis of the diffraction peaks was performed using PANalytical X´pert HighScore software.

3. Results and discussion

3.1 Chemistry of the activation process

Fig. 1 depicts the evolution of mass spectrometric signals with temperature, corresponding to the main compounds released during the thermal activation of the impregnated samples of bone char.

3.1.1 Release of aldehydes, HCN and cyanides

Fig. 2a and b show the evolution of the signals of HCN and cyanides, respectively. All samples, including the precursor, exhibit a well defined peak at temperatures between 300 and 600 ºC, with its maximum at around 500 ºC.

It should be noticed, though, that the signal of CN^- is a secondary signal of HCN. If HCN was the only source of CN^- ions, both signals should follow an invariable

HCN/CN^- ratio of 1:0.17 [23]. However, the measured HCN/CN^- intensity ratio is around 1:0.09 for all samples, which evidences the presence of CN^- in pyrolysis gases.

Robau-Sánchez et al. [19] reported the formation of cyanides during the activation with KOH of a carbonaceous material (Quercus agrifolia char). These authors proposed alternative mechanisms which result in the formation of cyanides in either liquid or gas form:

$$6\ KOH\ (l) + 5.5\ C + N_2\ (g) \leftrightarrow 2\ KCN\ (l) + 2\ K_2CO_3 + 1.5\ CH_4\ (g) \quad (1)$$

$$6\ KOH\ (l) + 5.5\ C + N_2\ (g) \leftrightarrow K_2(CN)_2\ (g) + 2\ K_2CO_3 + 1.5\ CH_4\ (g) \quad (2)$$

Liquid cyanides might then be transformed into gaseous cyanides:

$$2KCN\ (l) \leftrightarrow K_2(CN)_2\ (g) \quad (3)$$

The essential condition for cyanide formation is the presence of carbon and nitrogen. Carbon represents about 10 wt% of bone char [6], and it contains also a small amount of structural nitrogen [24]. Thus, the cyanide formation evidences that structural nitrogen took part in the activation process, probably following a reaction pathway similar to that described by Eq. (1)-(2).

Regarding the formation of HCN during the pyrolysis, there could be two possibilities: (i) its direct synthesis, following a mechanism similar to that mentioned before, or (ii) its synthesis from cyanides, through the reaction of these components with H_2O and CO_2, H_2O or acids:

$$2\ NaCN + H_2O + CO_2 \leftrightarrow Na_2CO_3 + 2\ HCN \quad (4)$$

$$KCN + H_2O \leftrightarrow HCN + KOH \quad (5)$$

$$CN^- + H^+ \leftrightarrow HCN \quad (6)$$

The above-mentioned set of equations involves the reaction of OH^- ions and consequently, it could be extended to every compound containing OH^- functionalities. In the case of BCO, there are two potential sources of OH^-: (i) the P-OH functionalities of HAP and (ii) the reaction of $CaCO_3$ constituent of bone char with water, according to Eq. (7) and (8) [25]:

$$CO_3^{2-} + H_2O \leftrightarrow HCO_3^- + OH^- \quad (7)$$

$$HCO_3^- \leftrightarrow CO_2 + OH^- \quad (8)$$

Eq. (7), which takes place at temperatures in the 200-600 ºC range, requires a source of water. As discussed below, the dehydration of hydroxyapatite in that temperature range results in a continuous release of water (Fig. 5).

The aforementioned mechanism is supported by the increased release of CN^- observed for alkali treated samples (BCN and BCK) as compared to non-chemically treated sample (BCO). For BCK, the large amount of CO_3^{2-} ions incorporated with K_2CO_3 leads to the formation of OH^- ions (Eq. (7)-(8)).

It is noteworthy the opposite behaviour of both acid treated samples, suggesting that different reaction pathways occur by either H_2SO_4 or H_3PO_4 activation. The sample treated with H_2SO_4 shows the lowest release of CN^-, slightly lower than the precursor itself. This fact could be ascribed to the partial dissolution of HAP, which leads to the formation of calcium sulphate and cation deficient HAP, $Ca_{10-X}(HPO_4)_X(PO_4)_{6-X}(OH)_{2-X}$ [25]. Cation deficient HAP, which contains a lower amount of P-OH functionalities, would result in a lower formation of cyanides.

BCP sample, on the contrary, shows the highest release of cyanides, an increase of 99% compared to BCO. This unexpected behaviour (given that this sample should have a lower amount of OH^- functionalities, due to its partial dissolution) could be related to the incongruent dissolution of HAP with H_3PO_4 and the formation of an amorphous structure. Fig. 9 shows the XRD patterns of the precursor, BCO, BCS and BCP samples, after being pyrolysed at 800 ºC. It is clear that the acid activation with phosphoric acid results in an important reduction of crystallinity, since only a wide band, different from those of HAP, is observed. Several authors have reported the dissolution of HAP with H_3PO_4. According to Krupa-Zuczek et al. [26], mild concentrations of acid would lead to the partial dissolution of HAP, resulting in a solid phase composed of HAP and $CaPO_3(OH)\cdot 2H_2O$. Other authors have reported the presence of various phosphates ($CaHPO_4\cdot 2H_2O$, $Ca(H_2PO_4)_2\cdot H_2O$ and $Ca_3(PO_4)_2$), after acid and heat treatment [27]. The wide band observed in the XRD pattern (in the 20-30º range) could be ascribed to the coalescence of those peaks.

According to this hypothesis, the aggressive treatment with H_3PO_4 would result in an amorphous, thermolabile structure, which would collapse during the pyrolysis step. A high amount of OH^- ions in the solid phase could then be released, thus being available to react according to Eq. (1)-(2).

The release of aldehydes occurs simultaneously to that of CN^- (Fig. 2c). Moreover, aldehydes follow a similar trend, given as follows: BCP >> BCK > BCN > BCO ≥ BCS. These results suggest that aldehydes are also formed through a mechanism which implies the reaction of carbon and hydroxides, which is in good agreement with their chemical formula (R-CHO).

To summarize, the following aspects could be highlighted, regarding the release of aldehydes, HCN and CN^-:

- The proposed reaction mechanism involves the reaction of C and OH^- ions (and structural N, in the case of HCN/CN^-).

- Since this mechanism implies the gasification of constituents of bone char (or incorporated species), it is expected to have an impact on the textural properties of the final material.

- The alkali treatment (with either NaOH or K_2CO_3) has the effect of incorporating OH^- ions, thus resulting in a higher extent of this set of reactions. Between both activation reagents, K_2CO_3 is more active.

- Acid treated samples show an opposite behaviour. The treatment with H_2SO_4 leads to the partial dissolution of HAP, resulting in a slightly lower release of aldehydes and HCN/CN^-. For the treatment with H_3PO_4, the formation of an amorphous and thermolabile structure is hypothesized. This structure would collapse during the thermal treatment, thus leaving a high amount of OH^- ions available to react according to the proposed mechanism.

3.1.2 Release of CH_4

All samples exhibit a peak of CH_4 starting around 400 ºC and with its maximum near 550 ºC (Fig. 3). The release of CH_4 is probably related to cyanide formation through Eq. (1)-(3), which involve the simultaneous formation of methane. This mechanism would be supported by the observed correlation between the intensity of CN^- and CH_4 signals for each sample (Fig. 2b and 3). However, an exception occurs with the sample activated with H_2SO_4, being the release of CH_4 higher than expected in that temperature range. This result evidences the occurrence of an additional mechanism of methane formation. It is likely that further amounts of CH_4 are formed through the methanation of CO_2 (Sabatier reaction, Eq. (9)) and CO (Eq. (10)):

$CO_2 + 4\ H_2 \leftrightarrow CH_4 + 2H_2O$ (9)

$CO + 3\ H_2 \leftrightarrow CH_4 + H_2O$ (10)

Both reactions have been reported in the gasification of carbonaceous materials, such as activated carbon [28] and rice straw [29] with CO_2 and steam. In this work, the intense release of CO and especially CO_2 around 550 ºC (and also the peak at higher temperature, around 850 ºC) observed for BCS (Fig. 4 and Fig. 7) strongly coincide with CH_4 release. These results support the occurrence of the above-mentioned methanation reactions. Furthermore, BCN and BCK also exhibit a minor peak of CH_4 (Fig. 1b and c) at high temperature (800-900 ºC), which is in good agreement with the small release of CO and CO_2 of these samples.

It is worth highlighting the following points concerning the evolution of methane:

- All samples show a peak with its maximum near 550 ºC, which could be related to the aforementioned mechanism of HCN/CN^- formation, that implies the simultaneous formation of methane.

- The release of CH_4 of the sample treated with H_2SO_4 (higher than expected at that temperature range, and with another peak at higher temperature) suggests the occurrence of an additional reaction mechanism, which is likely to be the methanation of CO and CO_2.

- Between both sets of reactions, that related to the formation of HCN/CN^- involves the gasification of constituents of bone char (or incorporated species). Methanation reactions, on the contrary, take place in gas phase and consequently, should not be related to the development of porosity.

3.1.3 Release of CO_2

All samples show a low and broad band of CO_2 in the 200-700 ºC range (Fig. 4). As mentioned before, in that temperature range carbonate ions present in bone char can react with water, according to Eq. (7). The resultant HCO_3^- ions and those contained in HAP crystals are then released as CO_2 and OH^-, as described by Eq. (8). It is noteworthy that the treatment with sulphuric acid results in a much greater release of CO_2 at mild pyrolysis conditions (200-700ºC). The reaction of H^+ ions with carbonates, promoting the formation of HCO_3^- ions (Eq. (11)) and their subsequent decomposition could explain this higher release of CO_2.

$$CO_3^{2-} + H^+ \leftrightarrow HCO_3^- \quad (11)$$

However, this behaviour is not observed for the sample treated with H_3PO_4. It is hypothesized that H_3PO_4 had a more destructive effect and, thus, a high amount of carbonates could have been removed during the impregnation step, prior to thermal activation.

Another characteristic feature of the sample activated with sulphuric acid is the formation of large quantities of CO_2 at high pyrolysis temperatures (between 700 and 1000 ºC) which is hardly observed for the other samples (Fig.1 and Fig. 4). This additional formation of CO_2, much higher than that observed at lower temperatures, should be attributed to specific reactions involving precursor constituents and H_2SO_4, rather than gas phase reactions, given that it is accompanied by a significant and rapid weight loss as observed in TG and DTG plots (Fig. 8). The source of carbon could be either the carbon contained within the precursor structure or $CaCO_3$, minor constituent of bone char (Eq. (12)-(13)). The thermodynamic analysis of these reactions has been conducted, taken into account the thermodynamic data of pure compounds [30]. According to our calculations, both reactions are spontaneous in the whole temperature range studied (Table 1).

$$2\ H_2SO_4 + C \leftrightarrow CO_2 + 2\ SO_2 + 2\ H_2O \quad (12)$$

$$H_2SO_4 + CaCO_3 \leftrightarrow CaSO_4 + CO_2 + H_2O \quad (13)$$

A similar set of reactions could be proposed for the activation with phosphoric acid:

$$4\ H_3PO_4 + 2\ C \leftrightarrow P_4O_6 + 2\ CO_2 + 6\ H_2O \quad (14)$$

$$2\ H_3PO_4 + 3\ CaCO_3 \leftrightarrow Ca_3(PO_4)_2 + 3\ CO_2 + 3\ H_2O \quad (15)$$

Eq. (14) is likely to be unfavourable ($\Delta G>0$). In fact, although no reliable data of entropy of formation of P_4O_6 could be found, the highly endothermic nature of the reaction (together with the absence of a well defined peak of CO_2 in the pyrolysis gases), suggests that this reaction does not take place.

Eq. (15), on the contrary, is spontaneous at the temperature range studied (Table 1). Nevertheless, the profile of CO_2 does not evidence the occurrence of this reaction during the thermal activation. There are two possible explanations: (i) that this reaction took place during the impregnation stage, prior to the pyrolysis, or (ii) that most carbonates were removed during the impregnation step (Eq. (11)), thus being

unavailable for Eq. (15). Fig. 10 exhibits the FTIR spectra of both the precursor (precarbonized sample) and BCO sample (non treated sample, after being thermally activated at 800 ºC). It is observed that both samples show a band at 1420–1463 cm^{-1}, corresponding to the C–O stretching mode of carbonate ions. It is noteworthy the absence of this band in the spectrum of BCP, which confirms the removal of carbonates during the treatment with H_3PO_4.

Another source of CO_2 at high temperature is the thermal decomposition of carbonates, both $CaCO_3$ constituent of bone char and those incorporated. It takes place at temperatures between 600-1000 ºC [31, 31, 31, 32]:

$$CaCO_3 \leftrightarrow CaO + CO_2 \quad (16)$$

$$K_2CO_3 \leftrightarrow K_2O + CO_2 \quad (17)$$

$$Na_2CO_3 \leftrightarrow Na_2O + CO_2 \quad (18)$$

A well defined peak of CO_2 (Fig. 1b and c) between 800 and 900 ºC is observed for samples BCN and BCK, which can be associated with their higher carbonate content. In the case of BCK, CO_3^{2-} ions are incorporated directly during the impregnation with K_2CO_3. Regarding the sample activated with NaOH, this release could be related to the formation of carbonates from the reaction of C and OH^-, following mechanisms similar to that previously mentioned, which involves Eq. (1)-(2).

The following aspects should be emphasized, concerning the release of CO_2:

- Carbonate ions react with water at 200-700 ºC to produce HCO_3^-, which is then decomposed releasing CO_2. The sample treated with H_2SO_4 exhibits a higher release, ascribed to the reaction of H^+ ions with carbonates, thus promoting the formation of HCO_3^-.

- BCS sample shows a high and rapid release of CO_2 at 700-1000 ºC, attributed to the reaction of H_2SO_4 with a source of carbon (structural carbon or CO_3^{2-}).

- The thermal decomposition of carbonates can hardly be observed. Only BCN and BCK samples exhibit a small peak at 800-900 ºC, which can be associated with their higher content of CO_3^{2-} ions, incorporated during the impregnation stage.

- Since all these reactions imply the gasification of several species, they are expected to have an impact on textural properties.

3.1.4 Release of H_2O

Curves of the release of H_2O are shown in Fig. 5. All samples exhibit a small peak below 200 ºC, ascribed to the desorption of adsorbed water. This peak is more pronounced for sulphuric acid treated sample, due to its capability to remove structural water. At higher temperatures, BCO, BCK and BCN show a low and continuous release of water, mainly attributed to the elimination of the surface P-OH groups of HAP by dehydration, which takes place in the 300-700 ºC range [33]:

$$2\ P{-}OH \leftrightarrow P{-}O{-}P + H_2O\ (g) \quad (19)$$

On the contrary, both acid activated samples exhibit a much larger release of H_2O, starting at around 300 ºC and reaching its maximum intensity at 450-500 ºC. This release of water could be attributed not only to the elimination of surface P-OH groups, but also to the formation of cation-deficient HAP ($Ca_{10-X}(HPO_4)_X(PO_4)_{6-X}(OH)_{2-X}$) during the chemical activation step. Cation deficient HAP is characterized by a Ca/P ratio lower than the stoichiometric value of 1.67. When heated at temperatures between 200-600 ºC its dehydration takes place through the following reaction [34]:

$$HPO_4^{2-} \leftrightarrow \frac{1}{2} P_2O_7^{4-} + \frac{1}{2} H_2O\ (g) \quad (20)$$

$P_2O_7^{4-}$ ions can subsequently react with OH^- at high temperature (700-800 ºC) [34]. Eq. (21) could be responsible for the shoulder around 750 ºC observed in water release pattern:

$$P_2O_7^{4-} + 2\ OH^- \leftrightarrow 2\ PO_4^{3-} + H_2O\ (g) \quad (21)$$

The intense release of water of acid treated samples beginning around 300ºC, attributed to the dehydration of HAP, is accompanied by a significant and rapid weight loss, as confirmed by TG and DTG plots (Fig. 8). It is evident that dehydration is strongly favoured by acid activation, since it promotes the formation of cation deficient HAP. The decrease in Ca/P ratio was confirmed by EDX analyses of the samples pyrolysed at 800 ºC: a Ca/P ratio of 1.64 was measured for the precursor and it dropped to 1.05 and 0.54 for BCP and BCS, respectively.

The lower Ca/P ratio of the sample treated with H_2SO_4 would result in a higher release of water, according to Eq. (20) and (21). Moreover, the reaction of sulphuric acid with structural carbon or carbonates would result in a higher concentration of water in

pyrolysis gases. As commented above, a high amount of water and CO_2 is released through Eq. (12) and (13). Part of this CO_2 can then undergo a transformation to either CH_4 (Eq. (9)) or CO (Eq. (25)), which also involve the formation of water. Fig. 5 reveals the more intense release of water corresponding to BCS.

Finally, the small peak of water observed at 800 ºC for sample BCN (Fig. 1b and Fig. 5) could be attributed to the decomposition of the incorporated hydroxides, as reported by others [17] and [35]:

$$2\ NaOH \leftrightarrow Na_2O + H_2O \quad (22)$$

Regarding the release of water, the following aspects should be taken into account:

- The desorption of adsorbed water takes place below 200 ºC.

- The dehydration of hydroxyapatite (attributed to the elimination of P-OH groups) occurs in the 300-700 ºC range.

- Acid activated samples exhibit a much larger release (with its maximum near 500 ºC), associated with the formation of cation-deficient HAP and its dehydration.

- All these reactions imply the gasification of several species and thus, should take part in pore generation.

3.1.5 Release of H_2

Fig. 6 depicts the evolution of the signal of H_2. It is observed that the release of hydrogen begins at 400 ºC for all samples, including the precursor. Lillo-Ródenas et al [16, 18] proposed the occurrence of a reaction mechanism that implies the release of H_2, during the chemical activation of anthracites with hydroxides:

$$6\ NaOH + C \leftrightarrow 2\ Na + 3\ H_2 + 2\ Na_2CO_3 \quad (23)$$

$$6\ KOH + C \leftrightarrow 2\ K + 3\ H_2 + 2\ K_2CO_3 \quad (24)$$

Based on our results, a reaction mechanism similar to that described by Eq. (23) and (24) might take place. This mechanism involves the reaction of OH^- ions with carbon. In the case of the precursor, the source of OH^- can be either the P-OH functionalities of HAP, or those OH^- ions formed from carbonates (Eq. (7) and (8)). Given that the impregnation with NaOH or K_2CO_3 results in a larger amount of OH^- ions, a higher release of hydrogen could be expected in the pyrolysis of these samples. Nevertheless, the opposite trend is observed. This fact could be explained by the occurrence of a

consecutive reaction, in which part of the hydrogen formed during the reaction of carbon and hydroxides would then react. This consecutive reaction, which would take place mainly at temperatures higher than 700 ºC, could be the reverse water gas shift reaction (RWGS) (Eq. (25)). The RWGS reaction has been reported during the pyrolysis of carbonaceous precursors [28] and [29].

$$CO_2 + H_2 \leftrightarrow CO + H_2O \quad (25)$$

This reaction requires a source of CO_2. Nevertheless, as mentioned before, except for BCS (and to a lesser extent, BCN and BCK), there is no evidence of CO_2 release. It is hypothesized, though, that the conversion of CO_2 into CO leads to its absence in pyrolysis gases, since as discussed in section 3.1.3, the release of CO_2 at 600-1000 ºC is well documented. The rapid transformation of CO_2 into CO, according to the RWGS reaction, would explain both the absence of CO_2 (Fig. 4) and the drop off in H_2 release at around 700 ºC (Fig. 6). This hypothesis is also supported by the role of K and Na as promoters of the RWGS reaction [28], [36], [37] and [38]. Thus, samples containing these alkali metals would lead to a higher depletion of hydrogen compared to the precursor (Fig. 6).

It is remarkable that the release of H_2 of BCS is much lower than that of BCO. This behaviour cannot be explained only by the reduction in the amount of OH^- functionalities (Eq. (23)-(24)), as a consequence of the partial dissolution of hydroxyapatite. As previously commented, CO_2 can react to produce either CO (RWGS reaction, Eq. (25)) or CH_4 (Sabatier-based methanation reaction, Eq. (9)). At low CO_2 concentrations (as occurred for all samples except for BCS (Fig. 4)), it would rapidly react through the RWGS reaction to produce CO. At larger concentrations, as for BCS, simultaneous methanation reactions are expected to occur, resulting in a great H_2 consumption.

The release of hydrogen was dramatically increased by treatment with H_3PO_4. This production of hydrogen should be ascribed to Eq. (23)-(24), involving the reaction of OH^- functionalities, along with the partial dissolution of HAP. According to the aforementioned hypothesis, the aggressive treatment with H_3PO_4 would lead to the formation of a non-crystalline and thermolabile structure. This structure would decompose during the thermal treatment, thus releasing a high amount of OH^- ions,

being available to react with carbon to produce H_2. The high release of hydrogen supports this hypothesis.

Regarding the evolution of H_2, the following aspects should be emphasized:

- The proposed mechanism for the formation of hydrogen involves the reaction of C and OH^- ions. Since this mechanism implies the gasification of constituents of bone char (or incorporated species), it is expected to have an impact on the development of porosity.

- For BCP sample, the release of a huge amount of H_2 is explained by the formation of an amorphous and thermolabile structure. This structure would collapse during the thermal treatment, thus leaving a high amount of OH^- ions available to react.

- Part of the H_2 formed reacts through a consecutive reaction, which could be mainly the rapid RWGS reaction (favoured by the presence of alkali metals). Another reaction pathway that leads to the depletion of hydrogen is the methanation reaction (which is of great importance in the case of BCS sample, due to the high release of CO_2). These consecutive reactions occur in gas phase and consequently, do not generate porosity.

3.1.6 Release of CO

Curves of CO release are shown in Fig. 7. All samples, including the precursor, show two peaks. The first peak appears in the 300-600 ºC range, with its maximum around 500 ºC. CO is likely to be formed from CO_2, via the RWGS reaction (Eq. (25)) as previously commented. The profile of CO_2 corresponding to this temperature range (Fig. 4) is in good agreement with that of CO. Moreover, every sample shows a clear peak of CO at a temperature range of 600-1000 ºC which should not be exclusively ascribed to RWGS reaction, as there is no direct relationship between the evolution of H_2 and CO for different samples. This result suggests the occurrence of an additional reaction mechanism for the production of CO above 700 ºC.

This reaction mechanism is likely to involve the gasification of carbon, constituent of bone char. Two reactions could take place in the gasification process. On the one hand, the reverse Boudouard reaction, in which CO_2 reacts with carbon to produce CO:

$$CO_2 + C \leftrightarrow 2\ CO \qquad (26)$$

Many authors have reported the occurrence of this reaction at temperatures above 700 ºC in the gasification of carbonaceous materials such as graphite [39] and MBM [40].

On the other hand, water vapour reacts with carbon to produce CO (water-gas reaction):

$$H_2O + C \leftrightarrow CO + H_2 \quad (27)$$

Ren et al. [24] studied the gasification behaviour of MBM char with steam at temperatures in the 850-1000 ºC range, and concluded that this carbonaceous material has higher gasification reactivity than several types of coal.

The derivative of the measured weight loss (Fig. 8b) supports the above mechanism in which structural carbon is converted into gaseous CO. The order in weight loss (BCS >> BCK > BCN > BCP ≈ BCO) mostly coincides with CO release (BCS >> BCK > BCP > BCN > BCO). It should be noticed, though, that the weight loss of BCS should not be ascribed only to this mechanism, but also to the reaction of H_2SO_4 with carbon or carbonates (Eq. (12)-(13)).

Gasification reactions (Eq. (26)-(27)) require a source of CO_2 and H_2O, respectively. In the case of acid activation (BCP, BCS), the formation of cation-deficient HAP and the reaction of carbon with sulphuric acid (Eq. (12)-(13)) are the main source of H_2O and CO_2 at high temperature. Consequently, it is expected that these samples give way to a higher release of CO than the precursor.

Regarding alkali activation (BCN, BCK), CO_2 is mainly released through the thermal decomposition of structural carbonates or those added by the activating agent. Moreover, it would also lead to an increased presence of H_2O in pyrolysis gases (Eq. (7), (8) and (22)), compared to BCO. It is well known the catalytic role of alkali metals such as K, Mg, Na and Ca for both the reverse Boudouard reaction, and the gasification of carbon with steam (Eq. (26)-(27)) [24] and [41], being K the most active [41]. Several authors proposed the mechanism described by Eq. (28), in which C acts as a reducing agent, to produce CO at temperatures above 700 ºC [42]. This reaction could also be extended to the sample treated with NaOH. The required oxides (K_2O and Na_2O) are likely to be formed through the aforementioned thermal decomposition of carbonates (Eq. (16)-(18)). Our results are in good agreement with these observations, since the CO formation of BCN and BCK was higher and shifted to a lower temperature than that of the precursor.

$$K_2O + C \leftrightarrow 2K + CO \quad (28)$$

It is worth highlighting the following points concerning the evolution of CO:

- The first release of CO (at 300-600 ºC) is attributed to the RWGS reaction (CO is formed from CO_2). This reaction takes place in gas phase, and thus, does not generate porosity.

- The peak of CO above 600 ºC could not only be attributed to RWGS reaction. The additional reaction mechanism is likely to be the gasification of carbon with CO_2 or H_2O, favoured by the presence of alkali metals (being K the most active). These gasification reactions are expected to develop the porous structure of the material.

3.2 Textural properties of the pyrolysed materials

The production yields and textural properties (surface area and pore volume) of the prepared samples of bone char are shown in Table 2. These values correspond to impregnated samples activated at 800 ºC. The production yield was maximum (21.5%) for the non-chemically treated sample (BCO). Alkali activation (samples BCN and BCK) did not further decrease the production yield, with values of 19.5 and 20.2%, respectively. On the contrary, acid activation significantly lowered the yield to 2.9 and 12.4%, by H_3PO_4 and H_2SO_4 activation, respectively.

The specific surface area and pore volume vary significantly depending on the activating agent used. It is noteworthy the extremely low value of surface area and pore volume of the sample treated with H_3PO_4. These results, which reveal that almost all the porous structure of the precursor was removed during the chemical activation, are in good agreement with the aforementioned hypothesis. According to this hypothesis, the aggressive treatment with phosphoric acid would incongruently dissolve HAP, resulting in the formation of an amorphous and thermolabile structure. This structure would be decomposed when heating, releasing high amounts of gases (such as H_2O, H_2 and CH_4), which would almost completely destroy the porous structure of HAP.

Regarding the alkali treated samples (BCN and BCK), an increase in the total surface area is observed, compared to BCO. Furthermore, a quite homogeneous increase in the micro- and mesoporosity (pore volume) is observed, whereas macroporosity remains almost constant. These textural properties must be related to the extent of the reactions which generate porosity, mainly: (i) those involving the reaction of C and OH^- ions, that generate compounds such as CN^- and aldehydes (Fig. 2b and c); and (ii) the gasification reactions of carbon (Eq. (26) and (27), Fig. 7), that generate CO. These reactions occur

in two temperature intervals: (i) 300-600 ºC: synthesis of CN^-/HCN and aldehydes; and (ii) 600-1000 ºC: gasification of carbon. The release of H_2 takes place in both temperature intervals (Figure 6), although it becomes more important at temperatures higher than 600 ºC.

Between both sets of reactions, that implying the reaction of structural C and OH^- ions to produce CN^-/HCN and aldehydes is of greater importance, since it gives way to a higher weight loss (Fig. 8b). Table 3 shows the released amounts of aldehydes and CN^-/HCN (calculated by integration), to be used as an indicator of the extent of this set of reactions. Fig. 11 displays the relationship between the released amount of CN^-/HCN and the pore volume of the sample. A similar figure is obtained when the amount of aldehydes is displayed. It is observed that there is a direct relationship between the extent of the reactions (BCK > BCN > BCO) and the development of micro- and mesoporosity, while macroporosity remains constant. This enhancement of porosity gives way to a significant increase in surface area, measured by S_{total} (59% for BCN and 74% for BCK).

Concerning the set of reactions occurring at temperatures above 600 ºC, the simultaneous occurrence of the RWGS reaction (Eq. (25)) makes it difficult to measure the amount of CO or H_2 effectively produced in gasification reactions. Thus, mass change in this temperature interval has been selected as an indicator of the extent of this set of reactions (Table 3). The extent of these reactions (BCK > BCN > BCO) is in good agreement with both the extent of the first set of reactions, and the development of micro- and mesoporosity (Table 2). Thus, it is clear that the effect of both alkali reagents is to favour the reactions that generate porosity (in the micro- and mesopore range) in the whole temperature range, being K_2CO_3 more active.

This homogeneous increase of micro- and mesoporosity results in a hierarchical porous material, with an excellent potential for applications as electrode material, in gas storage, catalysis, and energy storage. Samples of bone char prepared by alkali treatment could be used as electrode materials for electric double-layer capacitor EDLC. According to the work of Wang et al. [43] ion-buffering reservoirs can be formed in the macropores to minimize the diffusion distances to the interior surfaces, the mesoporous walls provide low-resistant pathways for the ions through the porous particles, and the micropores strengthen the electric double layer capacitance. Consequently, the

combination of micro-, meso- and macroporous structures helps to maintain a good capacitive behaviour of the resultant material.

Furthermore, the great increase in specific surface area allows the chemical activation with NaOH and K_2CO_3 to be considered as a suitable method to improve the performance of HAP as a catalytic support. Its desirable properties, i.e. structural stability, ion-exchange ability, acid-base properties and adsorption capacity, make HAP a promising material to configure heterogeneous catalysts. HAP-based catalysts have been recently employed in some chemical transformations, such as the oxidation of alcohols to aldehydes [44] or the oleic acid esterification [7].

Finally, the sample treated with H_2SO_4 shows a completely different trend in the development of porosity (Fig. 11), which cannot be mainly ascribed to the aforementioned reactions of carbon with OH^- to produce compounds such as CN^-/HCN and aldehydes. According to the data of Table 2, BCS sample exhibits a remarkable increase of microporosity (135%, compared to BCO), while the macropore volume dramatically decrease (65%). Moreover, there is a trade-off between external and micropore area, since total area hardly varies. This decrease is mainly due to the reduction in macroporosity, since mesopore area remains almost constant.

The development of microporosity should then be attributed to specific reactions involving H_2SO_4. Among the reactions which could have an impact on textural properties, two should be highlighted, according to their relative importance (measured by weight loss intensity and velocity in the TG and DTG plots, Fig. 8): the dehydration of cation-deficient HAP (Eq. (20)-(21)), and the reaction of H_2SO_4 with a source of carbon (Eq. (12)-(13). This selective development of microporosity results in a material suitable to be used in gaseous pollutant adsorption, to remove compounds such as SO_2 [45] or VOCs [46].

4. Conclusions

When studying the development of porosity during the chemical activation of bone char, it is essential to distinguish between gasification reactions (which result in weight loss) and reactions in gas phase, which not generate porosity. Gasification processes involve the thermal decomposition or the reaction of constituents of bone char (hydroxyapatite, carbonates, carbon, nitrogen) and those compounds incorporated in the impregnation stage.

The mechanisms to generate porosity are: (i) the desorption of adsorbed water; (ii) those involving the reaction of carbon and OH^- ions, which produce compounds such as CN^-, HCN, aldehydes and H_2; (iii) the thermal decomposition of carbonates; (iv) the gasification of carbon with CO_2 or H_2O; (v) the dehydration of HAP or cation-deficient hydroxyapatite; and (vi) the reaction of H_2SO_4 with carbon or carbonates.

The mechanisms through which each activation agent enhances the development of porosity depend on the nature of the agent. Acids lead to the formation of cation deficient HAP, which is strongly dehydrated under thermal treatment. Furthermore, H_2SO_4 readily reacts with carbon. The main effect of alkali treatment (with NaOH or K_2CO_3) is the incorporation of OH^- ions, which can then react with carbon. Other reaction pathways favoured are the thermal decomposition of carbonates and the gasification of carbon, promoted by alkali metals.

The treatment with H_2SO_4 produces a highly microporous material, given that there is a trade-off between pores in the macropore and micropore range. Alkali treatment, on the contrary, results in a more equilibrated increase of micro- and mesoporosity, with no variation in the macropore range. Between both agents, the effect of K_2CO_3 is more pronounced than that of NaOH.

Consequently, it is possible to choose the most appropriate treatment method to use, depending on the desired textural properties of the material. The selective development of microporosity allows the treatment with H_2SO_4 to be considered as a suitable method to configure a material to be used in gaseous pollutant adsorption, to remove compounds such as SO_2 or VOCs. Alkali treatment, on the contrary, results in a hierarchical porous material, with an excellent potential for applications as electrode, in gas storage, catalysis and energy storage.

Finally, under the operating conditions used in this work, the treatment with H_3PO_4 was extremely aggressive. Phosphoric acid is likely to incongruently dissolve HAP, forming an amorphous and thermolabile structure, which is decomposed by heating, leading to the formation of high amounts of gases, which would almost completely destroy the porous structure of HAP.

5. Acknowledgements

The authors wish to thank to the Basque Government (UFI 11/39 (UPV/EHU)) for their economic support.

References

1. O. Senneca, Characterisation of meat and bone mill for coal co-firing, Fuel 87 (2008) 3262-3270.

2. J.A. Conesa, A. Fullana, R. Font, Thermal decomposition of meat and bone meal, J. Anal. Appl. Pyrolysis 70 (2003) 619-630.

3. G. Skodras, P. Grammelis, P. Basinas, Pyrolysis and combustion behaviour of coal–MBM blends, Bioresour. Technol. 98 (2007) 1-8.

4. J.A. Conesa, A. Fullana, R. Font, Dioxin production during the thermal treatment of meat and bone meal residues, Chemosphere 59 (2005) 85-90.

5. E.J. Cummins, K.P. McDonnell, S.M. Ward, Dispersion modelling and measurement of emissions from the co-combustion of meat and bone meal with peat in a fluidised bed, Bioresour. Technol. 97 (2006) 903-913.

6. C.W. Cheung, C.K. Chan, J.F. Porter, G. McKay, Combined Diffusion Model for the Sorption of Cadmium, Copper, and Zinc Ions onto Bone Char, Environ. Sci. Technol. 35 (2001) 1511-1522.

7. R. Chakraborty, D. RoyChowdhury, Fish bone derived natural hydroxyapatite-supported copper acid catalyst: Taguchi optimization of semibatch oleic acid esterification, Chem. Eng. J. 215–216 (2013) 491-499.

8. R.M. Mohamed, E.S. Baeissa, Preparation and characterisation of Pd–TiO_2–hydroxyapatite nanoparticles for the photocatalytic degradation of cyanide under visible light, Applied Catalysis A: General 464–465 (2013) 218-224.

9. P.A. Goodman, H. Li, Y. Gao, Y.F. Lu, J.D. Stenger-Smith, J. Redepenning, Preparation and characterization of high surface area, high porosity carbon monoliths from pyrolyzed bovine bone and their performance as supercapacitor electrodes., Carbon 55 (2013) 291-298.

10. S.S.M. Hassan, N.S. Awwad, A.H.A. Aboterika, Removal of mercury(II) from wastewater using camel bone charcoal, J. Hazard. Mater. 154 (2008) 992-997.

11. E. Cascarosa, M.C. Ortiz de Zarate, J.L. Sánchez, G. Gea, J. Arauzo, Sulphur removal using char and ash from meat and bone meal pyrolysis, Biomass Bioenergy 40 (2012) 190-193.

12. S. Kongsri, K. Janpradit, K. Buapa, S. Techawongstien, S. Chanthai, Nanocrystalline hydroxyapatite from fish scale waste: Preparation, characterization and application for selenium adsorption in aqueous solution, Chem. Eng. J. 215–216 (2013) 522-532.

13. D. Pham Minh, N.D. Tran, A. Nzihou, P. Sharrock, Hydroxyapatite gel for the improved removal of Pb^{2+} ions from aqueous solution, Chem. Eng. J. 232 (2013) 128-138.

14. Ministerio de Agricultura, Alimentación y Medio Ambiente (Ministry of Agriculture, Food and Environment), Caracterización del Sector Porcino Español. Año 2012. Online 2014. http://www.magrama.gob.es/es/ganaderia/temas/produccion-y-mercados-ganaderos/Caracterizaci%C3%B3n_del_sector_porcino_2012_tcm7-310559.pdf

15. A.M. Puziy, O.I. Poddubnaya, A. Martínez-Alonso, F. Suárez-García, J.M.D. Tascón, Synthetic carbons activated with phosphoric acid III. Carbons prepared in air, Carbon 41 (2003) 1181-1191.

16. M.A. Lillo-Ródenas, D. Cazorla-Amorós, A. Linares-Solano, Understanding chemical reactions between carbons and NaOH and KOH: An insight into the chemical activation mechanism, Carbon 41 (2003) 267-275.

17. J. Guo, A.C. Lua, Textural and chemical characterisations of activated carbon prepared from oil-palm stone with H_2SO_4 and KOH impregnation, Microporous and Mesoporous Materials 32 (1999) 111-117.

18. M.A. Lillo-Ródenas, J. Juan-Juan, D. Cazorla-Amorós, A. Linares-Solano, About reactions occurring during chemical activation with hydroxides, Carbon 42 (2004) 1371-1375.

19. A. Robau-Sánchez, A. Aguilar-Elguézabal, J. Aguilar-Pliego, Chemical activation of Quercus agrifolia char using KOH: Evidence of cyanide presence, Microporous and Mesoporous Materials 85 (2005) 331-339.

20. E. Deydier, R. Guilet, S. Sarda, P. Sharrock, Physical and chemical characterisation of crude meat and bone meal combustion residue: “waste or raw material?”, J. Hazard. Mater. 121 (2005) 141-148.

21. M.T. Izquierdo, A. Martínez de Yuso, B. Rubio, M.R. Pino, Conversion of almond shell to activated carbons: Methodical study of the chemical activation based on an experimental design and relationship with their characteristics, Biomass Bioenergy 35 (2011) 1235-1244.

22. C. Moreno-Castilla, F. Carrasco-Marín, M.V. López-Ramón, M.A. Alvarez-Merino, Chemical and physical activation of olive-mill waste water to produce activated carbons, Carbon 39 (2001) 1415-1420.

23. B.B. Burton, A.R. Lavoie, S.M. George, Tantalum Nitride Atomic Layer Deposition Using (tert-Butylimido)tris(diethylamido)tantalum and Hydrazine, Journal of The Electrochemical Society 155 (2008) D508-D516.

24. H. Ren, Y. Zhang, Y. Fang, Y. Wang, Co-gasification behavior of meat and bone meal char and coal char, Fuel Process Technol 92 (2011) 298-307.

25. A. Yasukawa, K. Kandori, T. Ishikawa, TPD-TG-MS Study of Carbonate Calcium Hydroxyapatite Particles, Calcif. Tissue Int. 72 (2003) 243-250.

26. K. Krupa-Żuczek, Z. Kowalski, Z. Wzorek, Manufacturing of phosphoric acid from hydroxyapatite, contained in the ashes of the incinerated meat-bone wastes, Polish Journal of Chemical Technology 10 (2008) 13-20.

27. M. Kon, L.M. Hirakata, Y. Miyamoto, F. Kawano, K. Asaoka, Surface-layer Modification of Hydroxyapatite Ceramic with Acid and Heat Treatments, Dent. Mater. J. 21 (2002) 170-180.

28. W. Chen, B. Lin, Hydrogen and synthesis gas production from activated carbon and steam via reusing carbon dioxide, Appl. Energy 101 (2013) 551-559.

29. B. Prabowo, K. Umeki, M. Yan, M.R. Nakamura, M.J. Castaldi, K. Yoshikawa, CO_2–steam mixture for direct and indirect gasification of rice straw in a downdraft gasifier: Laboratory-scale experiments and performance prediction, Appl. Energy 113 (2014) 670-679.

30. T.E. Daubert, R.P. Danner, Physical and Thermodynamic Properties of Pure Chemicals. Data Compilation., 5 ed., Taylor & Francis, Washington, 1994.

31. Y. Wang, W.J. Thomson, The effect of sample preparation on the thermal decomposition of $CaCO_3$, Thermochimica Acta 255 (1995) 383-390.

32. R.L. Lehman, J.S. Gentry, N.G. Glumac, Thermal stability of potassium carbonate near its melting point, Thermochimica Acta 316 (1998) 1-9.

33. H. Tanaka, T. Watanabe, M. Chikazawa, FTIR and TPD studies on the adsorption of pyridine, n-butylamineand acetic acid on calcium hydroxyapatite, J. Chem. Soc. , Faraday Trans. 93 (1997) 4377-4381.

34. J.A.S. Bett, L.G. Christner, W.K. Hall, Hydrogen held by solids. XII. Hydroxyapatite catalysts, J. Am. Chem. Soc. 89 (1967) 5535-5541.

35. T. Yang, A.C. Lua, Characteristics of activated carbons prepared from pistachio-nut shells by potassium hydroxide activation, Microporous and Mesoporous Materials 63 (2003) 113-124.

36. A. Bansode, B. Tidona, P.R. von Rohr, A. Urakawa, Impact of K and Ba promoters on CO_2 hydrogenation over Cu/Al_2O_3 catalysts at high pressure, Catal. Sci. Technol. 3 (2013) 767-778.

37. G. Jacobs, B.H. Davis, Surface interfaces in low temperature water-gas shift: The metal oxide synergy, the assistance of co-adsorbed water, and alkali doping, Int J Hydrogen Energy 35 (2010) 3522-3536.

38. C. Chen, W. Cheng, S. Lin, Study of reverse water gas shift reaction by TPD, TPR and CO_2 hydrogenation over potassium-promoted Cu/SiO_2 catalyst, Applied Catalysis A: General 238 (2003) 55-67.

39. N. Zong, Y. Liu, Learning about the mechanism of carbon gasification by CO_2 from DSC and TG data, Thermochimica Acta 527 (2012) 22-26.

40. C.G. Soni, Z. Wang, A.K. Dalai, T. Pugsley, T. Fonstad, Hydrogen production via gasification of meat and bone meal in two-stage fixed bed reactor system, Fuel 88 (2009) 920-925.

41. C.K. Acharya, F. Jiang, C. Liao, P. Fitzgerald, K.S. Vecchio, R.J. Cattolica, Tar and CO_2 removal from simulated producer gas with activated carbon and charcoal, Fuel Process Technol 106 (2013) 201-208.

42. M. Hunsom, C. Autthanit, Adsorptive purification of crude glycerol by sewage sludge-derived activated carbon prepared by chemical activation with H_3PO_4, K_2CO_3 and KOH, Chem. Eng. J. 229 (2013) 334-343.

43. D. Wang, F. Li, M. Liu, G. Lu, H. Cheng, 3D Aperiodic Hierarchical Porous Graphitic Carbon Material for High-Rate Electrochemical Capacitive Energy Storage, Angewandte Chemie 120 (2008) 379-382.

44. W. Amer, K. Abdelouahdi, H. Ramananarivo R., M. Zahouily, E. Mokhtar Essassi, A. Fihri, A. Solhy, Oxidation of Benzylic Alcohols into Aldehydes Under Solvent-Free Microwave Irradiation Using New Catalyst-Support System, Current Organic Chemistry 17 (2013) 72-78.

45. N. Karatepe, İ. Orbak, R. Yavuz, A. Özyuğuran, Sulfur dioxide adsorption by activated carbons having different textural and chemical properties, Fuel 87 (2008) 3207-3215.

46. R.R. Gil, B. Ruiz, M.S. Lozano, M.J. Martín, E. Fuente, VOCs removal by adsorption onto activated carbons from biocollagenic wastes of vegetable tanning, Chem. Eng. J. 245 (2014) 80-88.

Table list

Figure captions

Fig. 1. Intensity of mass spectrometric signals of the compounds released during the pyrolysis. a) BCO. b) BCN. c) BCK. d) BCP. e) BCS.

Fig. 2. Ion current of several species as a function of pyrolysis temperature for all samples of bone char. a) m/z = 27 (HCN). b) m/z = 26 (CN^-). c) m/z = 29 (aldehydes)

Fig. 3. Ion current of m/z = 16 (CH_4) as a function of pyrolysis temperature for all samples of bone char.

Fig. 4. Ion current of m/z = 44 (CO_2) as a function of pyrolysis temperature for all samples of bone char.

Fig. 5. Ion current of m/z = 18 (H_2O) as a function of pyrolysis temperature for all samples of bone char.

Fig. 6. Ion current of m/z = 2 (H_2) as a function of pyrolysis temperature for all samples of bone char.

Fig. 7. Ion current of m/z = 12 (CO) as a function of pyrolysis temperature for all samples of bone char.

Fig. 8. Pyrolysis of samples of bone char under nitrogen atmosphere. a) TG curves. b) DTG curves, including the main reactions which lead to weight loss in each region.

Fig. 9. XRD patterns for the precursor (precarbonized sample), and BCO, BCS and BCP samples after being pyrolysed at 800 ºC.

Fig. 10. FTIR spectra of the precursor (precarbonized sample), and BCO, BCS and BCP samples after being pyrolysed at 800 ºC.

Fig. 11. Pore volume (in the micropore, mesopore and macropore range) as a function of the amount of CN^- and HCN released.

-

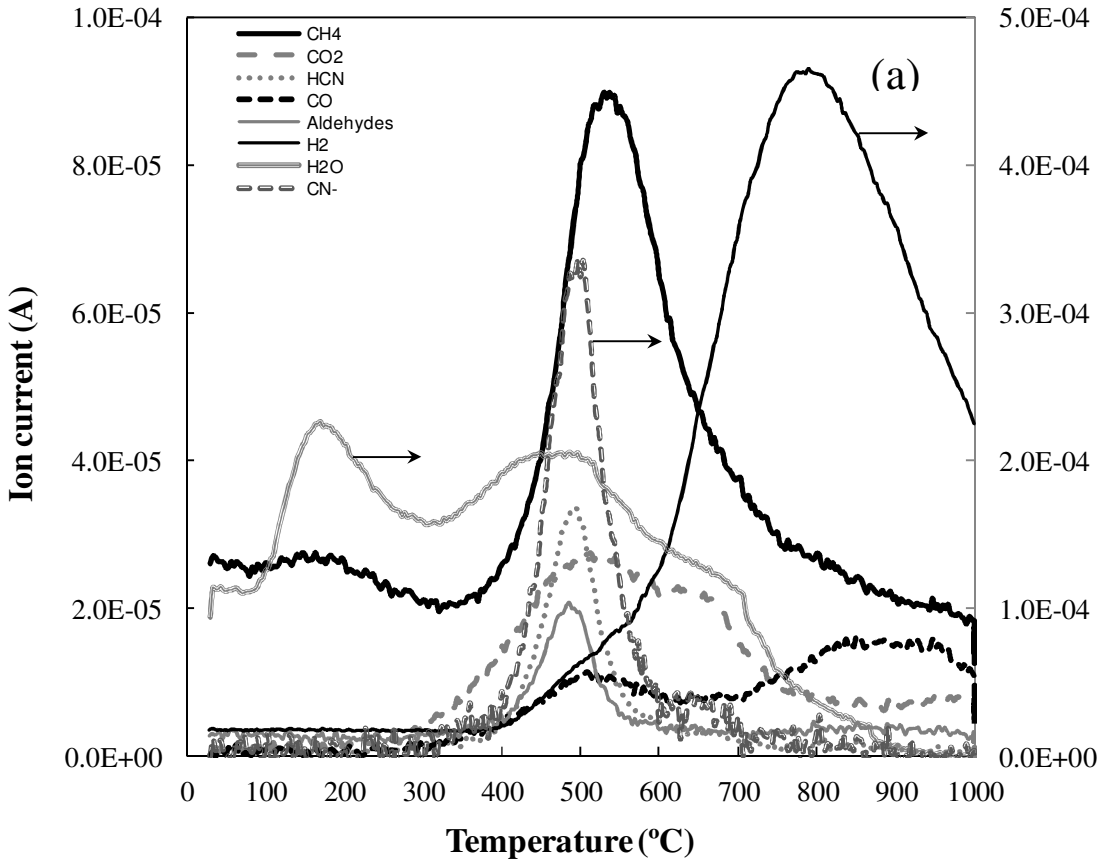
1.0E-04
8.0E-05
6.0E-05
4.0E-05
2.0E-05
0.0E+00
5.0E-04
4.0E-04
3.0E-04
2.0E-04
1.0E-04
0.0E+00
Ion current (A)
0
100
200
300
400
500
600
700
800
900
1000
Temperature (°C)
CH4
CO2
HCN
CO
Aldehydes
H2
H2O
CN-
(a)

Fig. 1a

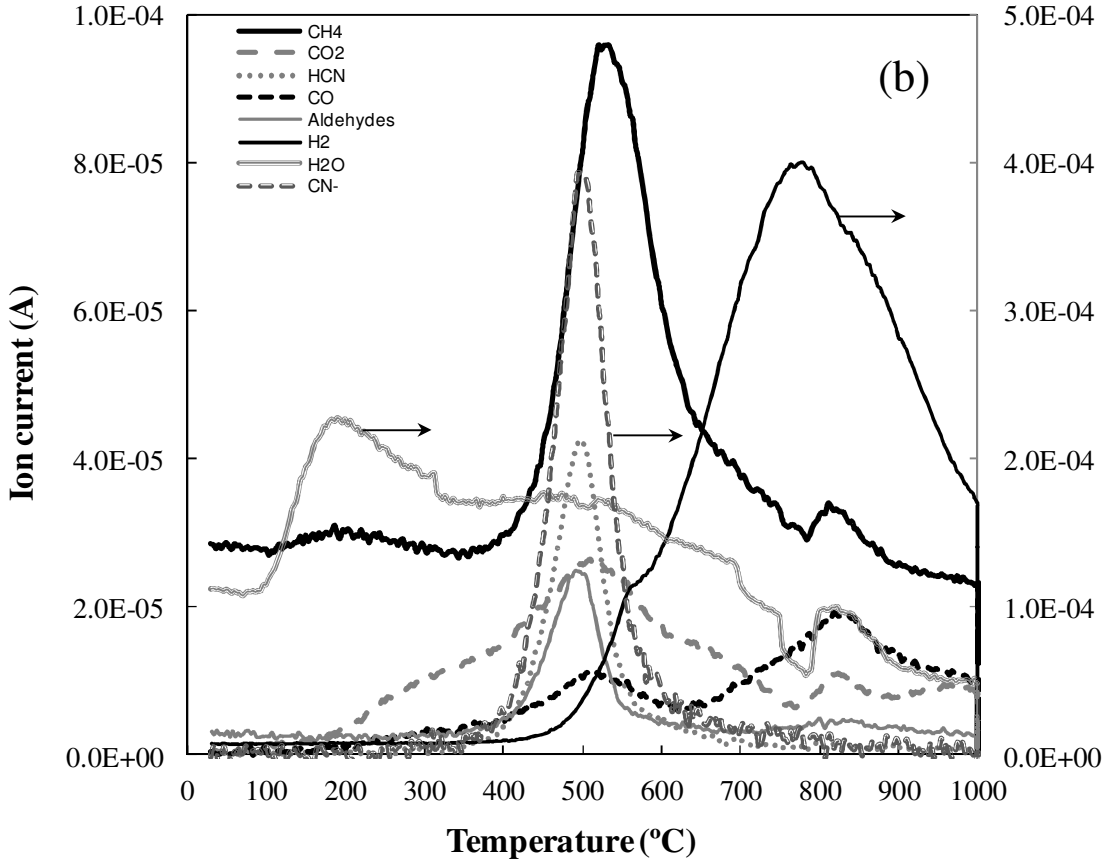
(b)
CH4
CO2
HCN
CO
Aldehydes
H2
H2O
CN-
Ion current (A)
Temperature (ºC)
1.0E-04
8.0E-05
6.0E-05
4.0E-05
2.0E-05
0.0E+00
5.0E-04
4.0E-04
3.0E-04
2.0E-04
1.0E-04
0.0E+00
0
100
200
300
400
500
600
700
800
900
1000

Fig. 1b

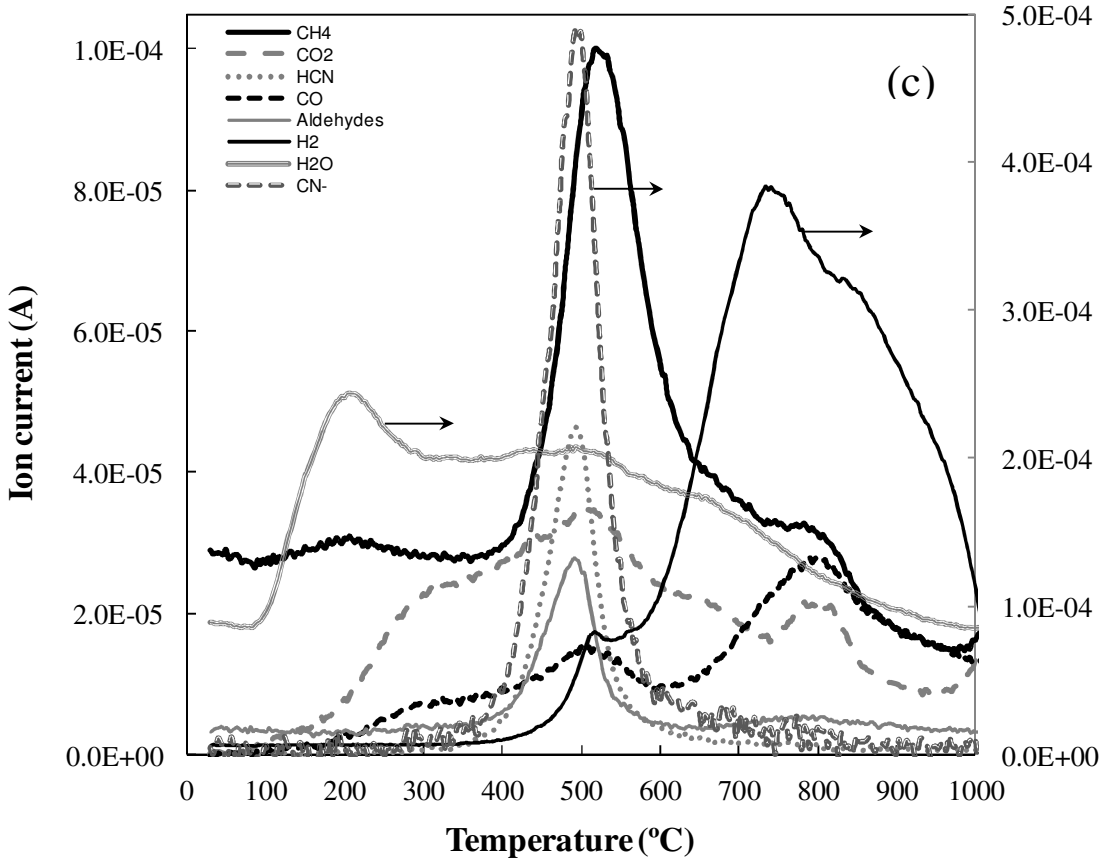
CH4
CO2
HCN
CO
Aldehydes
H2
H2O
CN-
(c)
Ion current (A)
1.0E-04
8.0E-05
6.0E-05
4.0E-05
2.0E-05
0.0E+00
5.0E-04
4.0E-04
3.0E-04
2.0E-04
1.0E-04
0.0E+00
0
100
200
300
400
500
600
700
800
900
1000
Temperature (ºC)

Fig. 1c

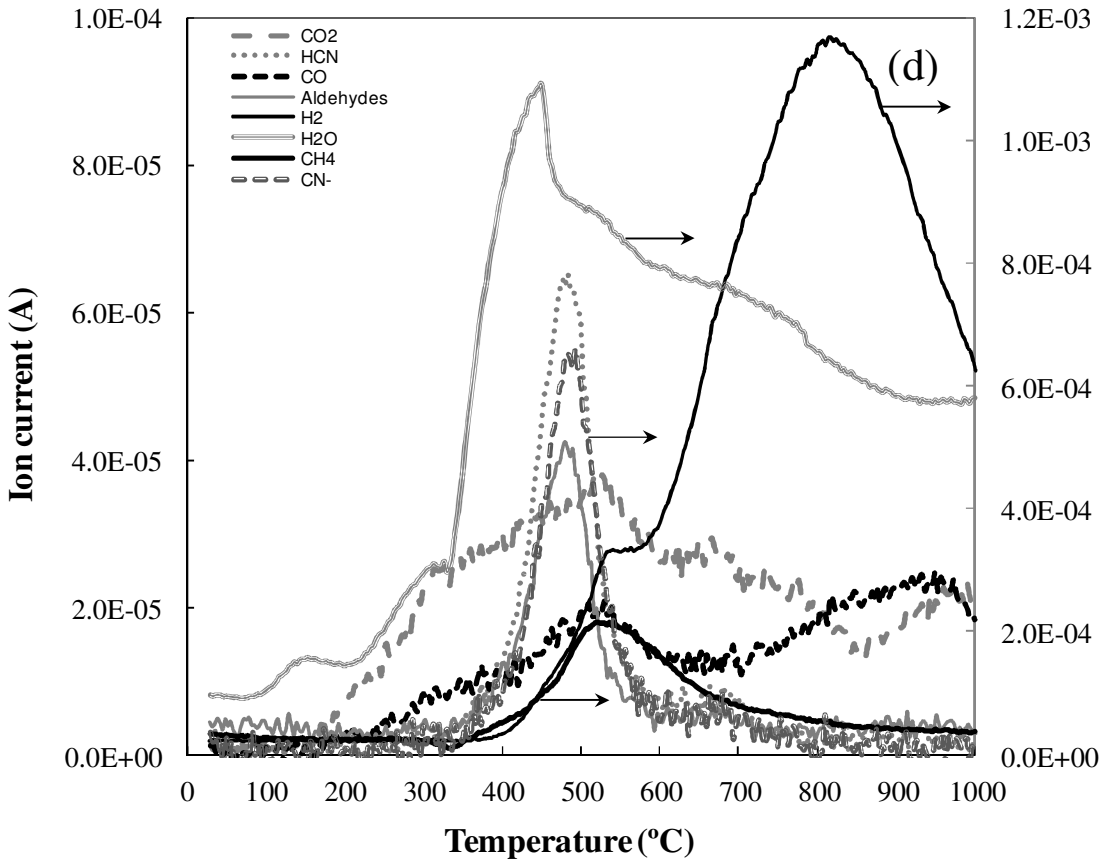
CO2
HCN
CO
Aldehydes
H2
H2O
CH4
CN-
(d)
Ion current (A)
1.0E-04
8.0E-05
6.0E-05
4.0E-05
2.0E-05
0.0E+00
1.2E-03
1.0E-03
8.0E-04
6.0E-04
4.0E-04
2.0E-04
0.0E+00
0
100
200
300
400
500
600
700
800
900
1000
Temperature (ºC)

Fig. 1d

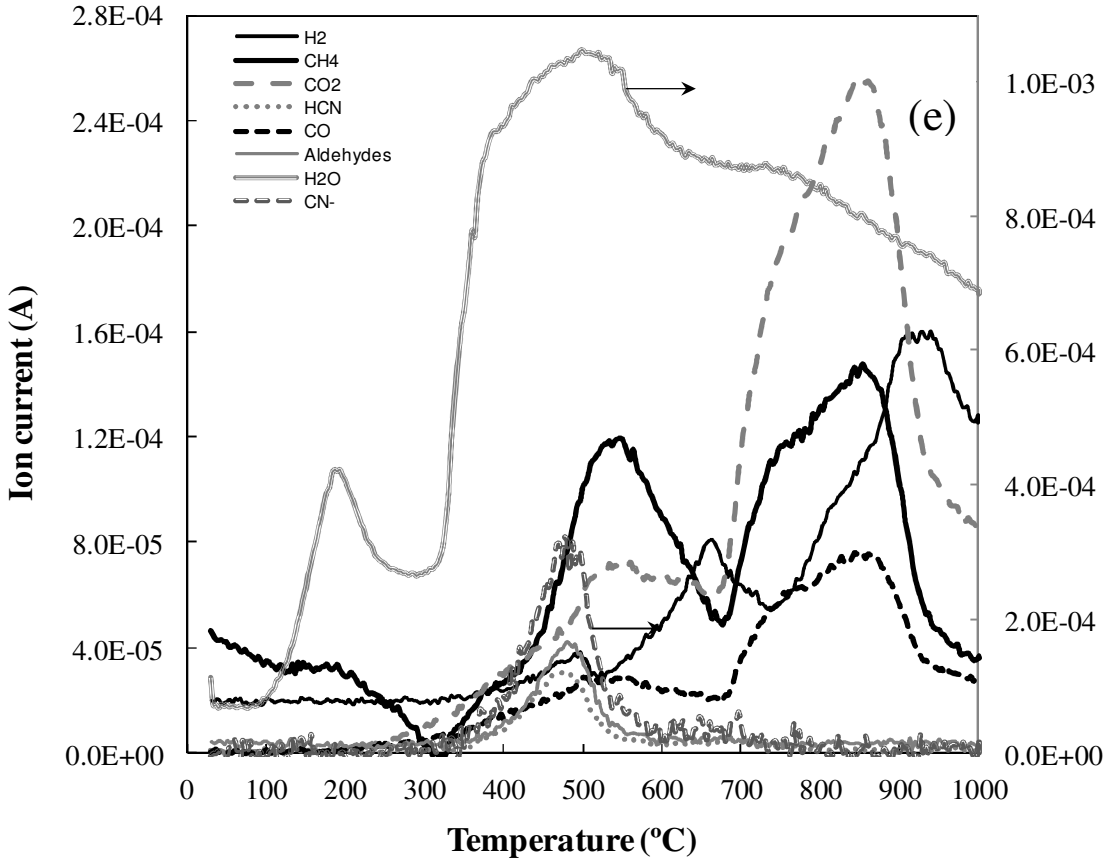
H2
CH4
CO2
HCN
CO
Aldehydes
H2O
CN-
(e)
Ion current (A)
2.8E-04
2.4E-04
2.0E-04
1.6E-04
1.2E-04
8.0E-05
4.0E-05
0.0E+00
1.0E-03
8.0E-04
6.0E-04
4.0E-04
2.0E-04
0.0E+00
0
100
200
300
400
500
600
700
800
900
1000
Temperature (ºC)

Fig. 1e

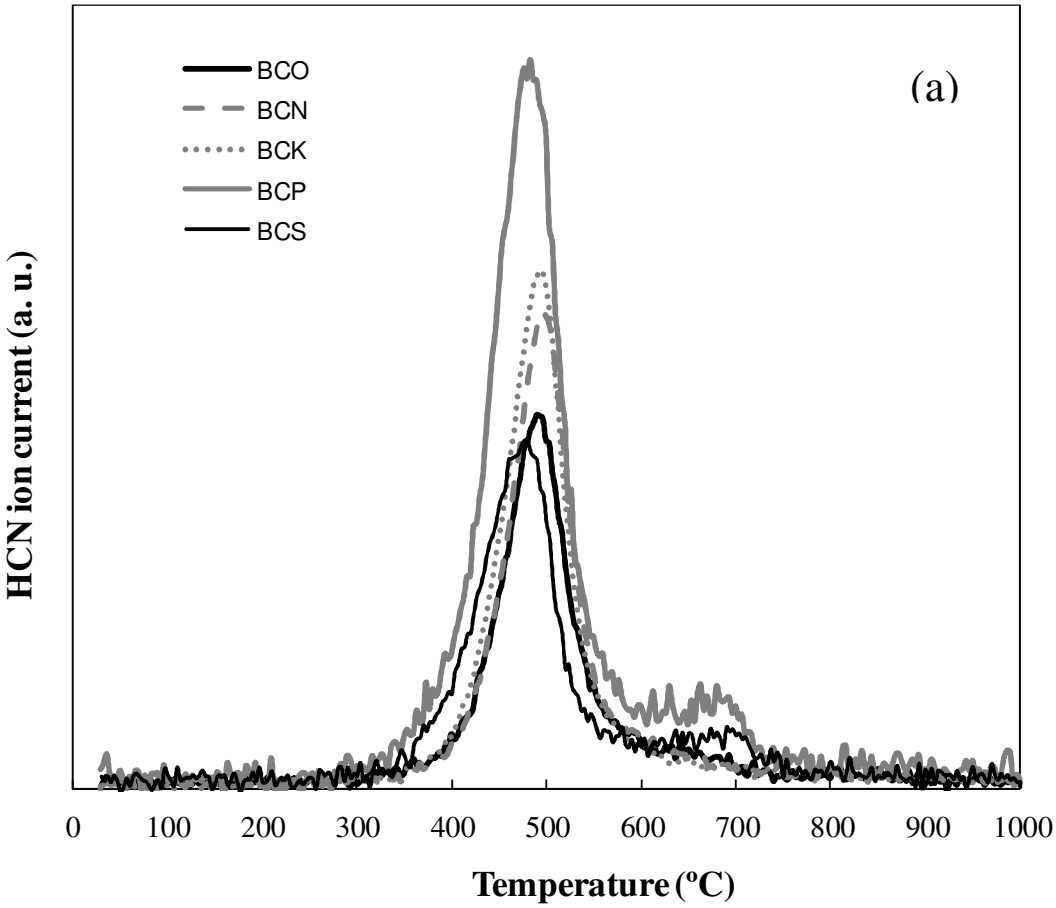
BCO
BCN
BCK
BCP
BCS
(a)
HCN ion current (a. u.)
0
100
200
300
400
500
600
700
800
900
1000
Temperature (°C)

Fig. 2a

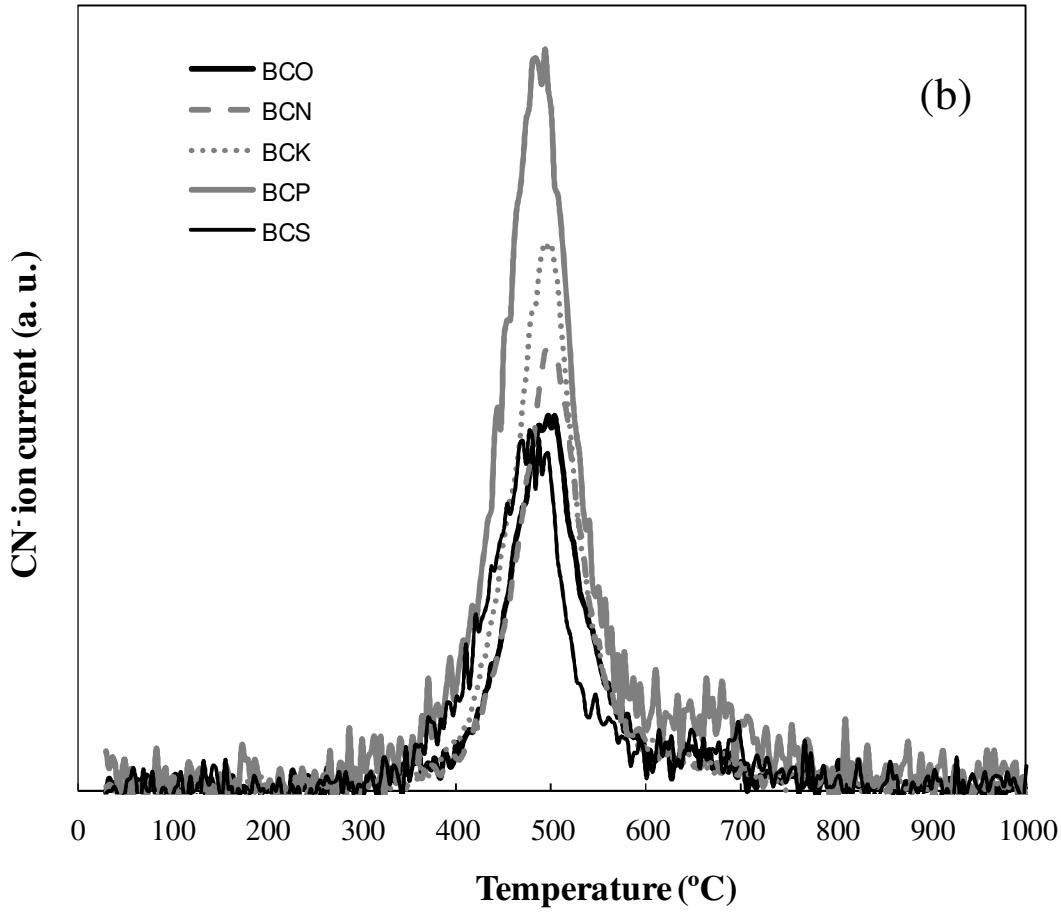
BCO
BCN
BCK
BCP
BCS
(b)
CN⁻ ion current (a. u.)
0
100
200
300
400
500
600
700
800
900
1000
Temperature (ºC)

Fig. 2b

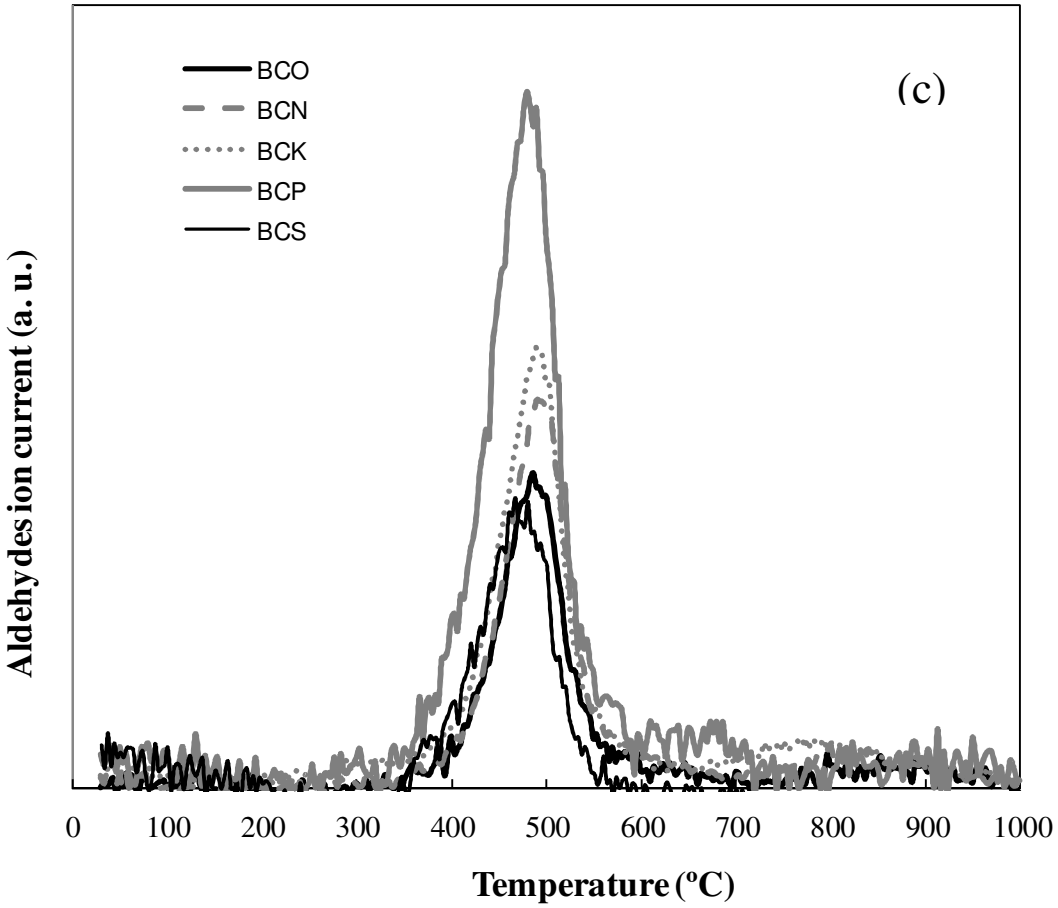
BCO
BCN
BCK
BCP
BCS
(c)
Aldehyde sion current (a. u.)
0
100
200
300
400
500
600
700
800
900
1000
Temperature (°C)

Fig. 2c

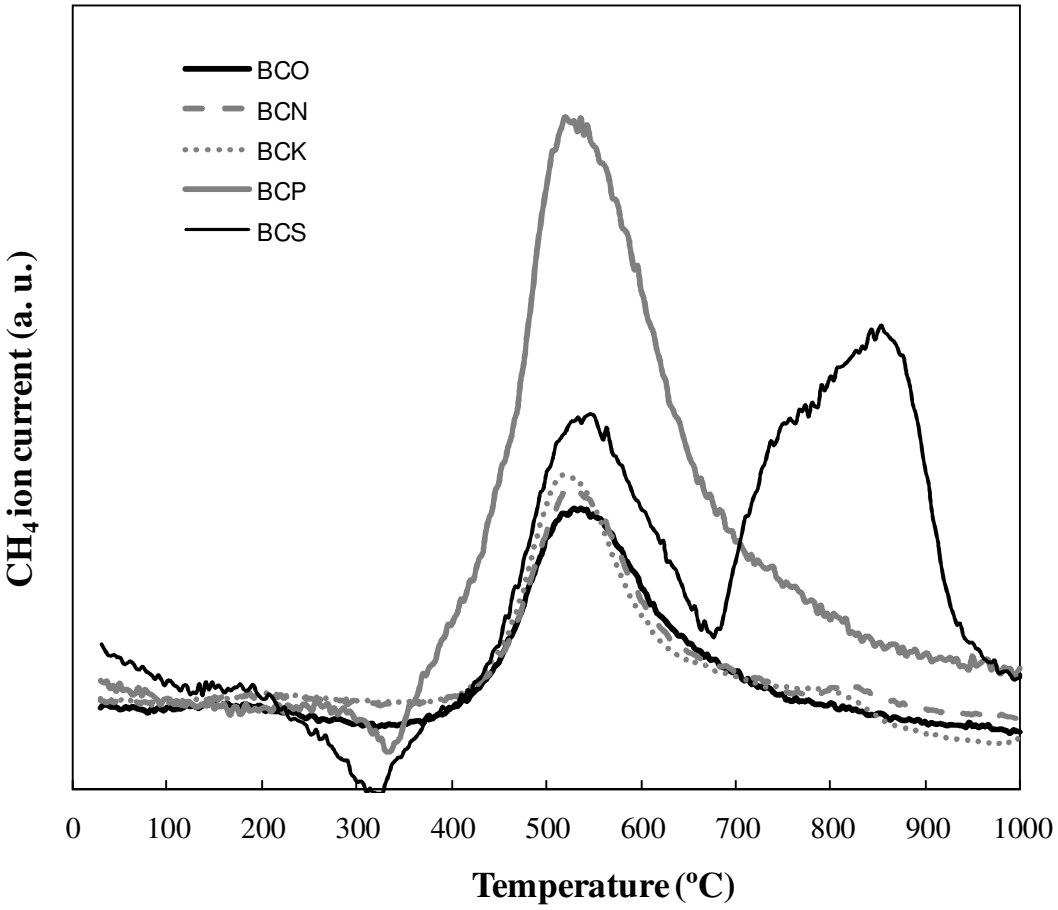
BCO
BCN
BCK
BCP
BCS
CH4 ion current (a. u.)
0
100
200
300
400
500
600
700
800
900
1000
Temperature (ºC)

Fig. 3

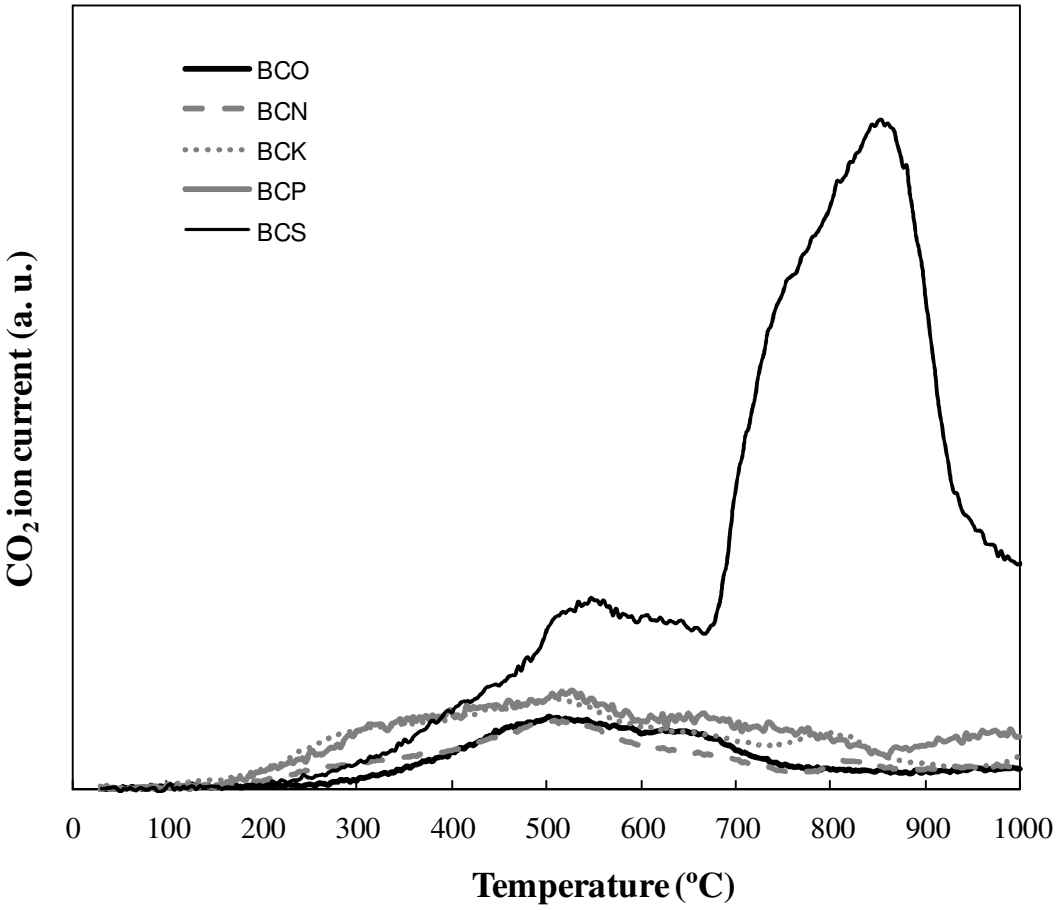
BCO
BCN
BCK
BCP
BCS
CO_2 ion current (a. u.)
0
100
200
300
400
500
600
700
800
900
1000
Temperature (°C)

Fig. 4

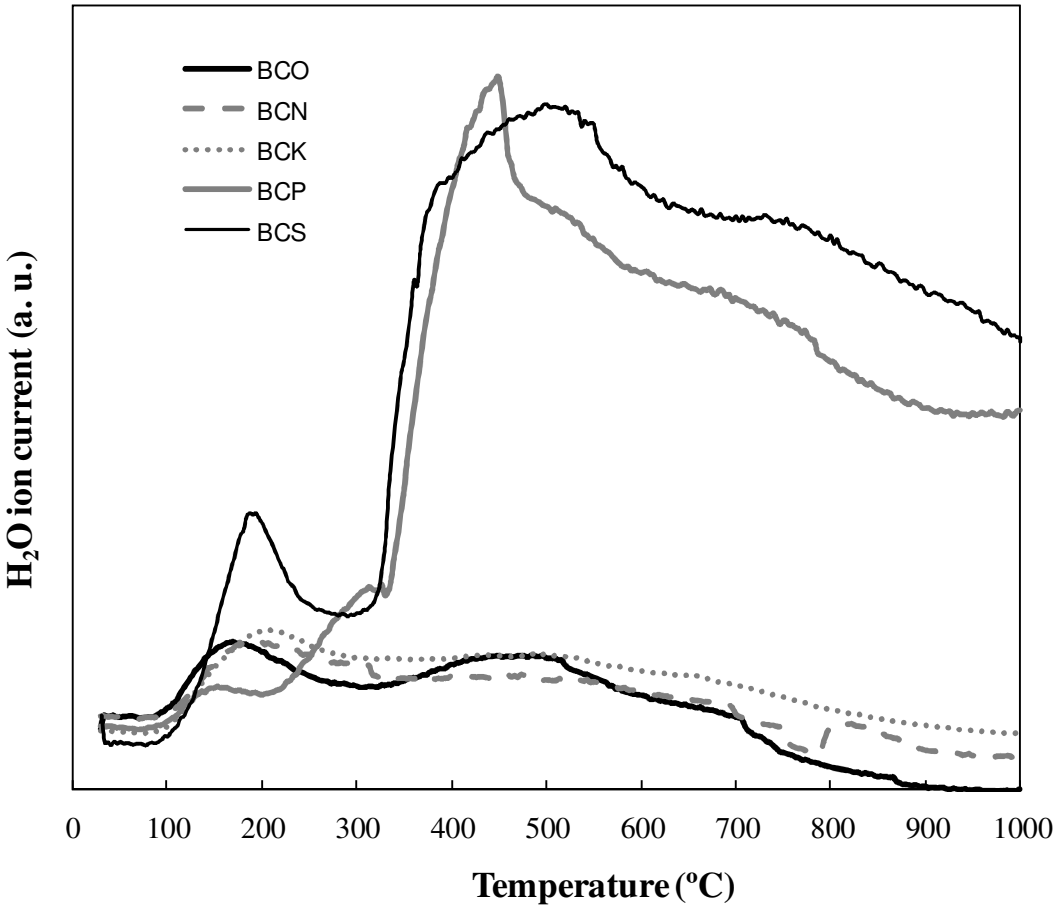
BCO
BCN
BCK
BCP
BCS
H2O ion current (a. u.)
0
100
200
300
400
500
600
700
800
900
1000
Temperature (ºC)

Fig. 5

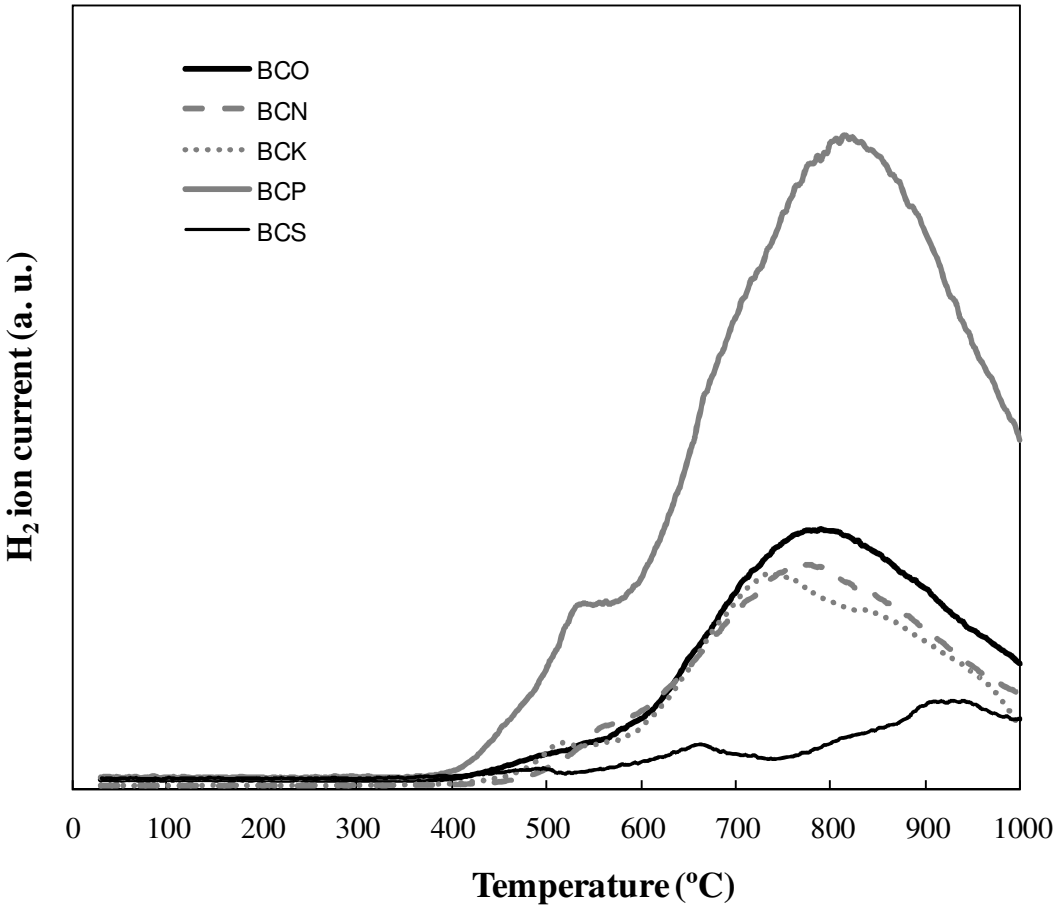
BCO
BCN
BCK
BCP
BCS
H2 ion current (a. u.)
0
100
200
300
400
500
600
700
800
900
1000
Temperature (ºC)

Fig. 6

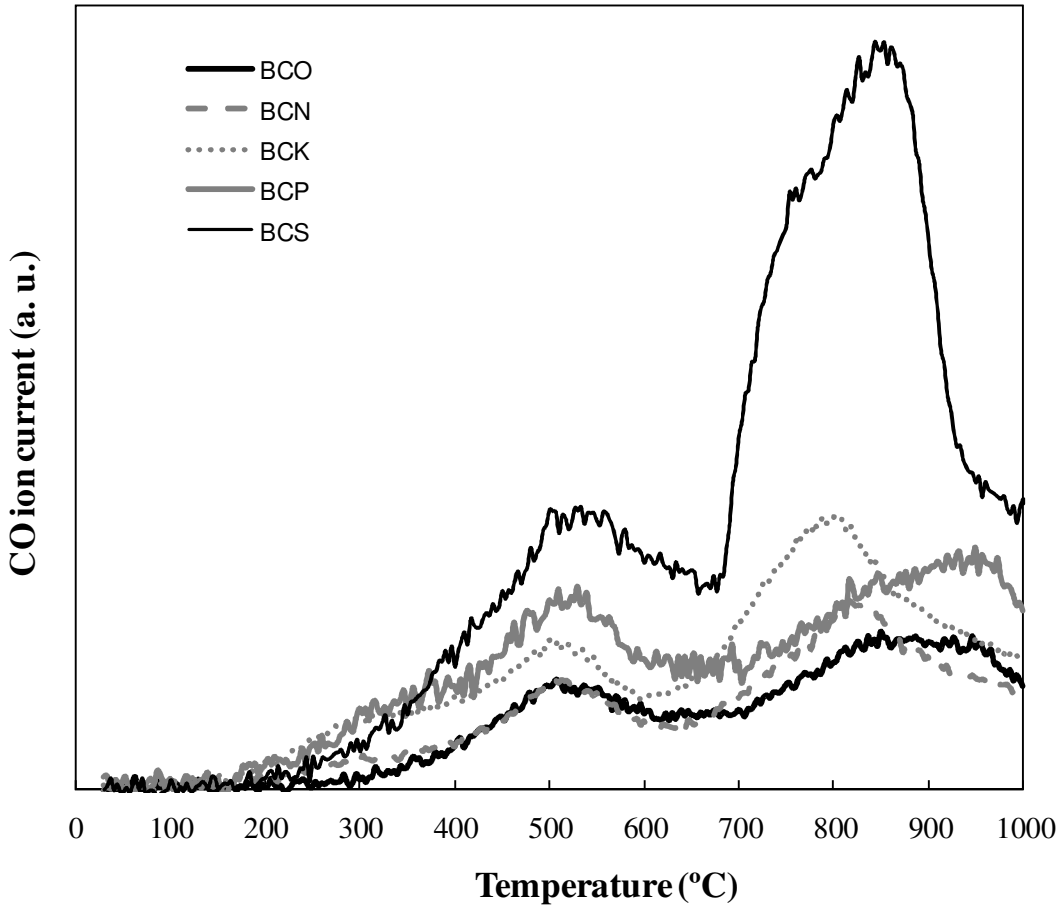
BCO
BCN
BCK
BCP
BCS
CO ion current (a. u.)
0
100
200
300
400
500
600
700
800
900
1000
Temperature (°C)

Fig. 7

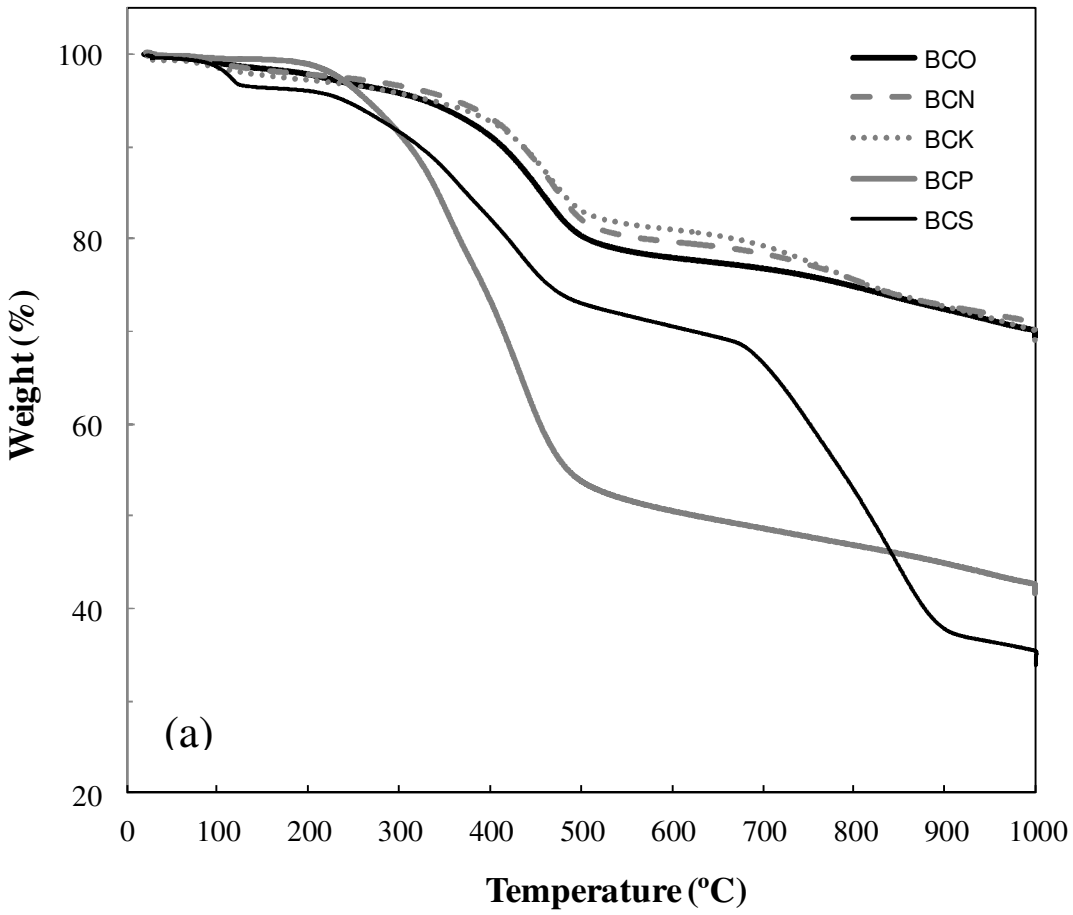
100
80
60
40
20
Weight (%)
0
100
200
300
400
500
600
700
800
900
1000
Temperature (ºC)
BCO
BCN
BCK
BCP
BCS
(a)

Fig. 8a

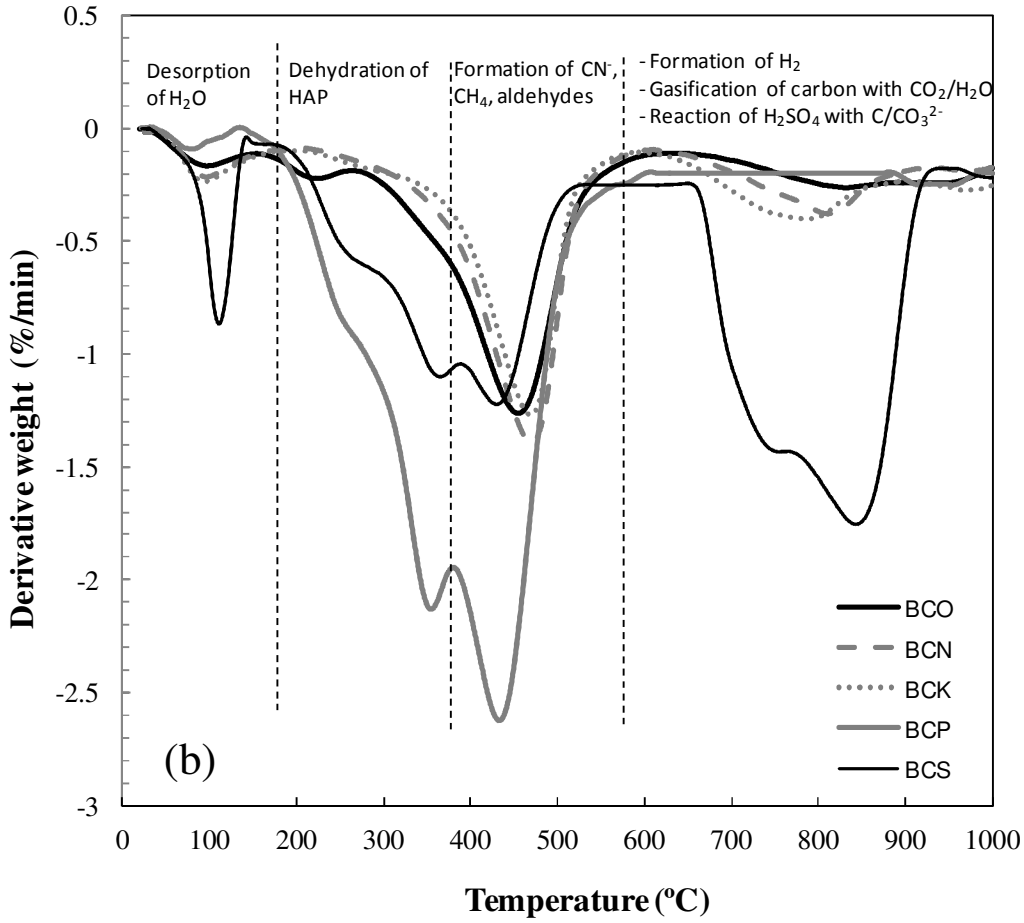
Desorption of H_2O
Dehydration of HAP
Formation of CN^-, CH_4, aldehydes
- Formation of H_2
- Gasification of carbon with CO_2/H_2O
- Reaction of H_2SO_4 with C/CO_3^{2-}
BCO
BCN
BCK
BCP
BCS
(b)
Derivative weight (%/min)
Temperature (°C)
0.5
0
-0.5
-1
-1.5
-2
-2.5
-3
0
100
200
300
400
500
600
700
800
900
1000

Fig. 8b

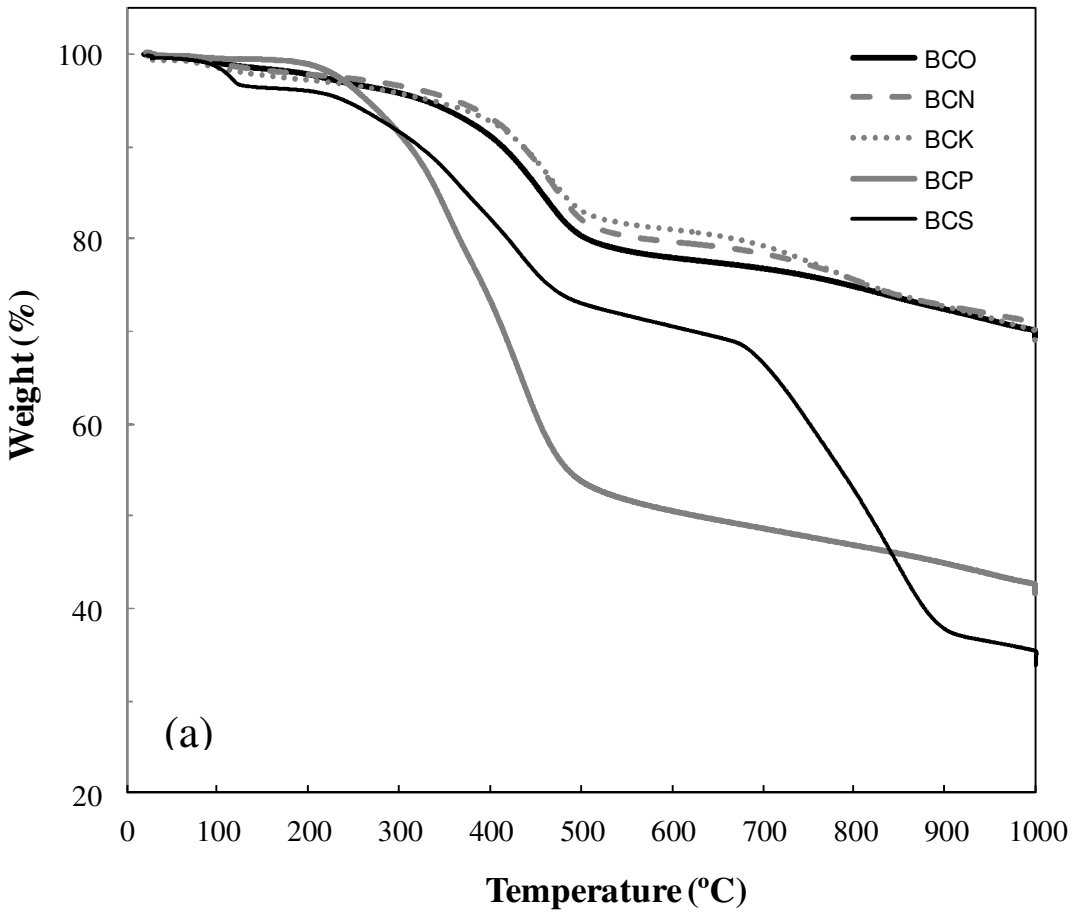
100
80
60
40
20
Weight (%)
0
100
200
300
400
500
600
700
800
900
1000
Temperature (ºC)
BCO
BCN
BCK
BCP
BCS
(a)

Fig. 8a

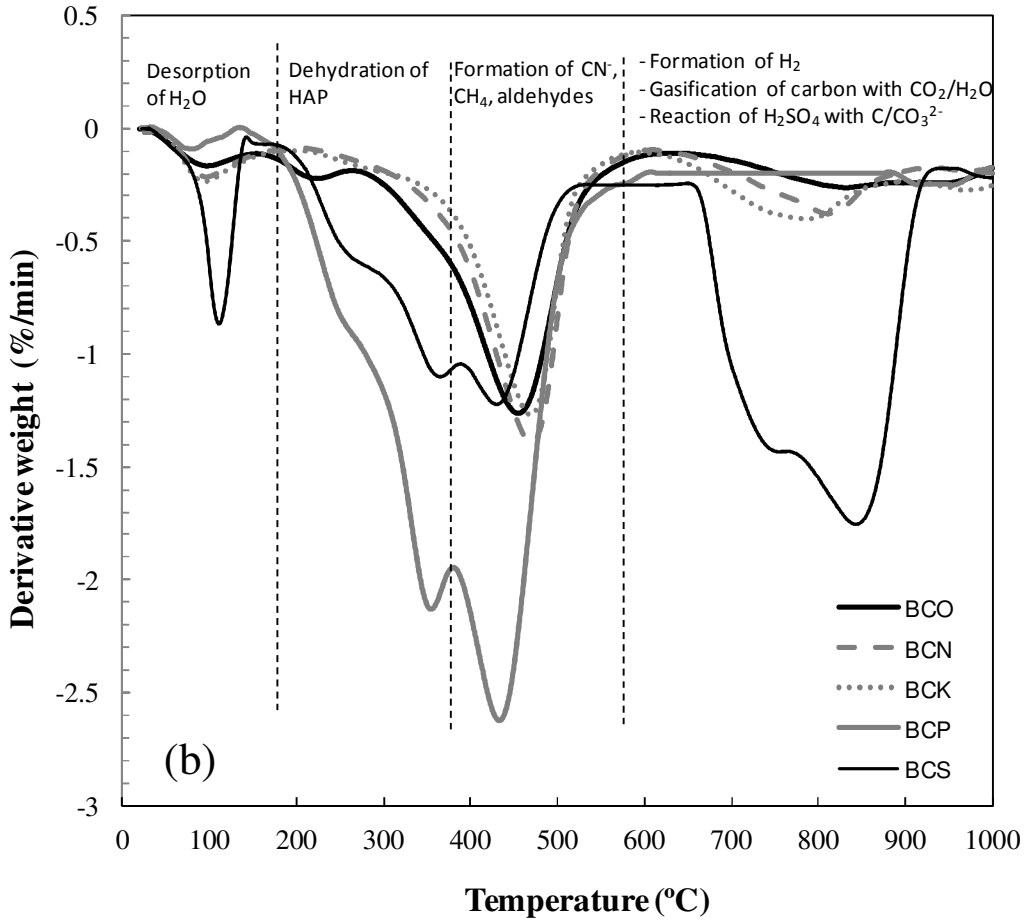
Desorption of H_2O
Dehydration of HAP
Formation of CN^-, CH_4, aldehydes
- Formation of H_2
- Gasification of carbon with CO_2/H_2O
- Reaction of H_2SO_4 with C/CO_3^{2-}
BCO
BCN
BCK
BCP
BCS
(b)
Derivative weight (%/min)
Temperature (°C)
0.5
0
-0.5
-1
-1.5
-2
-2.5
-3
0
100
200
300
400
500
600
700
800
900
1000

Fig. 8b

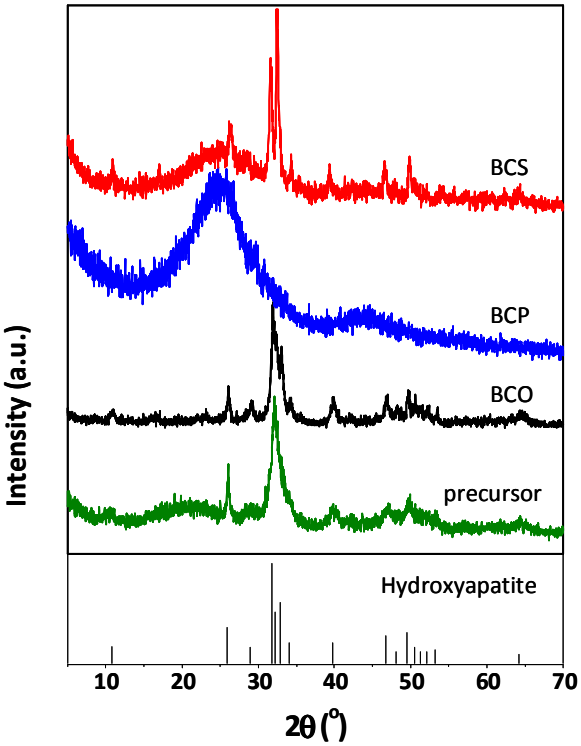
BCS
BCP
BCO
precursor
Hydroxyapatite
Intensity (a.u.)
10
20
30
40
50
60
70
2θ (°)

Fig. 9

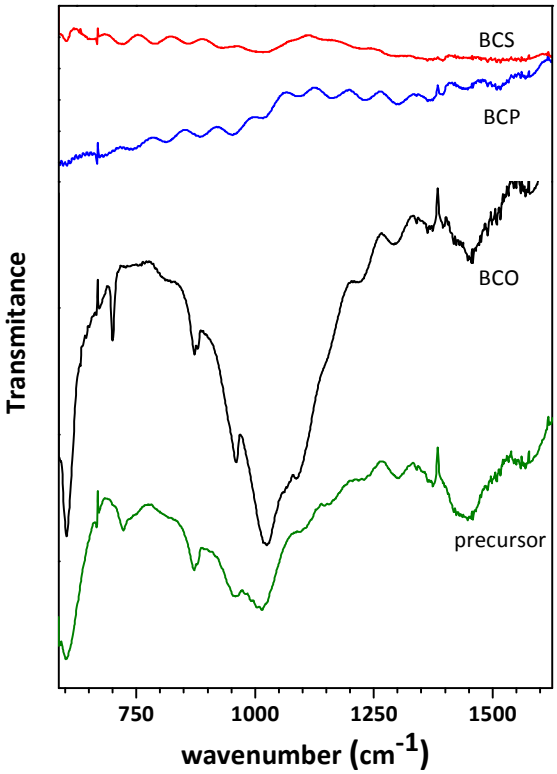
BCS
BCP
BCO
precursor
Transmitance
750
1000
1250
1500
wavenumber (cm-1)

Fig. 10

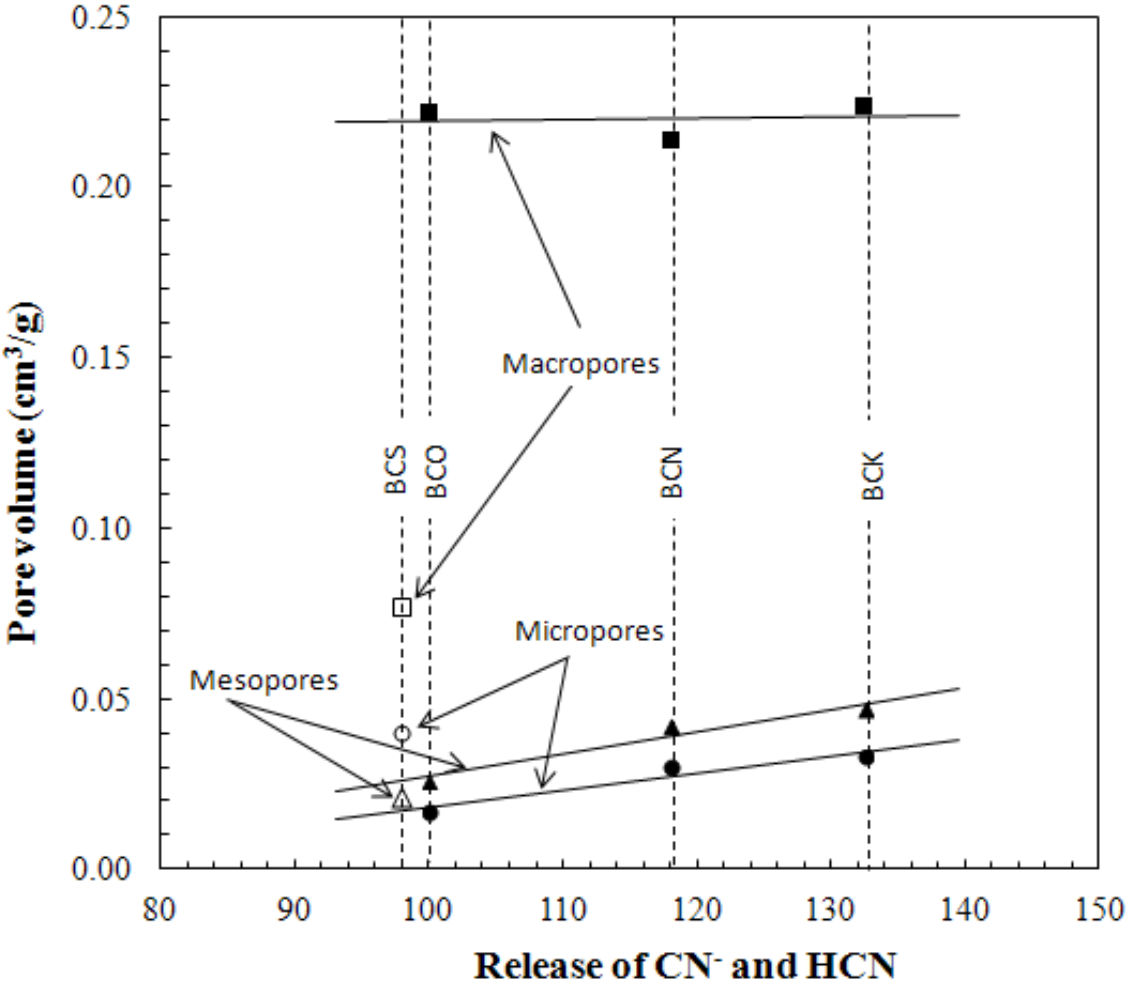
0.25
0.20
0.15
0.10
0.05
0.00
Pore volume (cm3/g)
80
90
100
110
120
130
140
150
Release of CN- and HCN
BCS
BCO
BCN
BCK
Macropores
Micropores
Mesopores

Fig. 11

Table 1. Standard enthalpy (kJ/mol) and entropy (kJ/mol K) changes, and Gibbs free energies (kJ/mol) for the proposed reactions between the acid reagent (H_2SO_4 or H_3PO_4) and the precursor.

Eq.	$\Delta H°$	$\Delta S°$	$\Delta G°$	ΔG (300 ºC)	ΔG (600 ºC)	ΔG (900 ºC)
(12)	-0.50	0.484	-144.8	-267.7	-386.0	-493.5
(13)	-127.3	0.120	-163.2	-191.3	-214.2	-231.9
(15)	85.8	0.872	-174.1	-412.2	-669.5	-925.0

Table 2. Production yields and textural properties of prepared samples of bone char.

Sample	Yield	S_{BET}	S_{micro} [a]	S_{meso} [b]	S_{macro} [b]	S_{total} [c]	V_{micro} [a]	V_{meso} [b]	V_{macro} [b]	V_{total} [c]
BCO	21.5	76.2	80	32	61	172.2	0.017	0.026	0.222	0.265
BCN	19.5	106.2	151	50	73	274	0.030	0.042	0.214	0.286
BCK	20.2	110.7	166	55	80	300	0.033	0.047	0.224	0.303
BCP	2.9	3.2	n.d.	4	1	4.7	n.d.	0.002	0.004	0.006
BCS	12.4	116.8	108	32	14	153.4	0.040	0.021	0.077	0.139

Surface area in m^2/g; pore volume in cm^3/g.

a DFT method
b BJH method
c Sum of DFT method (D_p<1.7 nm) and BJH method (D_p >1.7 nm)

Table 3. Released amounts of several compounds (calculated by integration), and mass loss in the 600-1000 ºC temperature range. For comparison purposes, a value of 100 has been assigned to BCO sample.

Sample	Aldehydes	CN^- + HCN	Mass loss 600-1000 ºC
BCO	100	100	100
BCN	122	118	113
BCK	139	133	134
BCS	94	98	508

HIGHLIGHTS

- A highly textured material, based mainly on HAP, was prepared from pork bone char.
- The reactions occurring during the chemical activation were investigated by TG-MS.
- Treatment with H_2SO_4 resulted in a highly microporous material.
- Treatment with NaOH and K_2CO_3 increased micro- and mesoporosity.
- These results are useful to configure a material with the desired textural properties